

Design and study of nanostructured coatings for the improvement of the corrosion resistance of aluminium alloys

Juan Deyo Maeztu Redin

Industrial Technologies Engineering

Advisors:

Pedro José Rivero Fuente Ph.D

Carlos Berlanga Labari Ph.D

IMEM Department, Universidad Pública de Navarra

Pamplona, June 2016

Acknowledgements

The realization of this project would not have been possible without the invaluable help and knowledge of Pedro José Rivero Fuente and Carlos Berlanga Labari, and the author would like to thank their patience and motivation. The author is also grateful to the Materials Laboratory team and all the Materials and Fabrication group of the Mechanics, Energy and Materials Engineering Department of the *Universidad Pública de Navarra*, for this opportunity and their priceless support. The author extends his sincere thanks to the Sensors Laboratory of the *Universidad Pública de Navarra*, for their professionalism and support, that has been immense. Thanks specially to *Nadetech Innovations* for their help and advice in operating their equipment and the AIN laboratories for the GDOES analyses. The author also thanks the Ministry of Economy and Competitiveness of the Spanish Government for funding this work through Project TRA2013-48603-C4-1-R.

To all of them and everybody that, one way or another, have made this possible, the author would like to express his sincerest and deepest gratitude.

¡Muchas gracias!

Abstract

This project consists of a comparative study of the corrosion behavior of different nanostructured coatings obtained by the combination of two different techniques. In the first one, sol-gel, alkoxides precursors are used to make different matrices depending on the control of aging time and number of dips. The second one, electrospinning, is used to make a fibrous coating of variable thickness controlling the viscosity, electrical potential, and flow collector distance. To evaluate the corrosion behavior, contact angle, Impedance Spectroscopy (EIS) and potentiodynamic polarization curves using assays (voltammetry) studies have been performed. In addition, the structure of the coatings obtained is evaluated by techniques of Glow discharge emission spectrometry (GDOES) and optical microscopy. Finally, the improvement of anticorrosive properties with an increase of the hydrophobicity of the coatings is also evaluated.

Extracto

El presente trabajo consiste en un estudio comparativo del comportamiento a corrosión de diferentes recubrimientos nanoestructurados obtenidos por la combinación de dos técnicas distintas. La primera de ellas, sol-gel, utiliza diferentes precursores alcóxidos para fabricar matrices en función del control del tiempo de envejecimiento y número de capas. La segunda, electrospinning, se utiliza para fabricar un recubrimiento de fibras de espesor variable controlando la viscosidad, potencial eléctrico, caudal y distancia de lanzado. Para evaluar el comportamiento a corrosión se realizan estudios de ángulo de contacto, Espectroscopía de Impedancias (EIS) y curvas de polarización mediante ensayos potenciodinámicos (voltametría). Además, se evalúa la estructura de los recubrimientos obtenidos mediante técnicas de Espectrometría de emisión de descarga luminiscente (GDOES) y microscopía óptica. Finalmente, se evalúa la mejora de las propiedades anticorrosivas con un aumento de la hidrofobicidad de los recubrimientos.

Contents

1. Corrosion: a brief introduction	1
1.1. Corrosion problems	1
1.2. Corrosion phenomena	2
1.3. Forms of corrosion	6
1.4. Corrosion prevention	10
2. Advanced coatings for corrosion protection of aluminium alloys	13
2.1. Aluminium alloys	13
2.1.1. Aluminium alloy 2024	14
2.2. Main conventional techniques and their drawbacks	16
2.2.1. Anodizing	16
2.2.2. Chrome plating	16
2.3. Sol-gel coatings	17
2.3.1. Sol-gel chemical principles	18
2.3.2. Sol-gel precursors	19
2.3.3. pH effects on sol-gel synthesis	21
2.3.4. Sol-gel deposition techniques	22
2.4. Hydrophobic coatings	23
2.4.1. Hydrophobic surfaces theory	23
2.4.2. Fabrication of hydrophobic surfaces	25
2.4.3. Hydrophobic coatings for corrosion protection	25
2.5. Electrospinning	27
3. Objectives	29
4. Methodology	31
4.1. Materials and equipment	31
4.1.1. Chemical substances	31
4.1.2. Equipment	33
4.2. Experimental procedure	35
4.2.1. Preparation of the surface of the aluminium samples	36
4.2.2. Sol-gel depositions by dip coating	38
4.2.3. Electrospinning deposition	39
4.2.4. Water contact angle measurement	39
4.2.5. Pitting corrosion tests	40
4.2.6. Electrochemical impedance spectroscopy test	41

5. Results	45
5.1. Experimental results data	45
5.1.1. Water contact angle measurement results	45
5.1.2. Pitting corrosion test results	47
5.1.3. Electrochemical impedance spectroscopy test results	49
5.1.4. Glow Discharge Emission Spectrometry results	66
5.2. Analysis and discussion of results	68
5.2.1. Number of dips	68
5.2.2. Heat treatment	70
5.2.3. Inhibitor	70
5.2.4. Hydrophobicity	72
5.2.5. Solubility of the electrospinning fibers	75
6. Conclusions and open research lines	77
Bibliography	79
Appendices	83
I. Appendix I: CNMAT 2016 poster	85
II. Appendix II: Equipment and chemicals data sheets	87

1. Corrosion: a brief introduction

1.1. Corrosion problems

The corrosion of metals represents an important problem for the modern societies. As it is recently estimated by the World Corrosion Organization, the annual direct cost of corrosion worldwide is greater than USD 1.8 trillion, more or less the 3-4% of the Gross Domestic Product (GDP). There are several studies about that costs in the United States [1], and the the Federal Highway Administration (FHWA) has estimated the direct cost of corrosion in the United States in \$U.S. 276 billion per year in 2001 (or 3.1% of the US GDP)[2]. There are not studies of that costs in Europe, but since the industrialization level is quite similar to that in the United States, similar values can be assumed. A 3.14% of the GDP of the Euro zone represents a cost of corrosion of 250 billion € [3], relatively large amount compared to the 133.8 billion € for the whole European Commission budget in 2009.

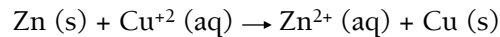
These values only take to account the direct costs associated to corrosion. Loss of production, environmental impacts, transportation failures, injuries and other indirect costs are estimated to be equal to the direct costs [3]. The total corrosion costs are assumed to be 6-8% of the GDP worldwide. It affects many areas and is a serious problem that affects the whole modern society.



Fig 1. Corrosion phenomena

1.2. Corrosion phenomena

The energy necessary to take an electron from a metal varies depending on the case: if two metals are in contact (e.g. zinc and copper), the copper will tend to get the electrons from the zinc. This is easily shown in the following experiment: when a zinc sheet is immersed in a copper (II) sulfate, the blue color of the sulfate solution starts to progressively disappear and the zinc sheet is covered by a reddish-black deposition of metallic copper, following this equation:



This is a spontaneous redox reaction in which an electron transfer occurs from the zinc to the copper ion. Each Cu^{2+} ion that deposits on the zinc sheet as a copper atom, takes two electrons from a zinc atom, that dissolves in form of Zn^{2+} ion. I.e., the zinc is oxidized and the copper is reduced. In this case, the electron transfer occurs directly between the atoms of zinc and the ions of copper, and no electric current can be obtained. However, an indirect delivery of the electrons can be forced by a conducting wire, obtaining an electric current. It is necessary to separate the Cu^{2+} ions (aq) from the direct contact with the zinc shell, so to prevent the direct electron transfer.

That is the basic principle of a galvanic cell, which is an apparatus that generates electricity through the use of a spontaneous reaction. It consists of a container with a zinc sheet (called the zinc electrode) immersed in a zinc sulfate solution (zinc electrolyte), and another container with a copper electrode immersed in a copper sulfate solution (copper electrolyte). The electrode in which oxidation occurs (zinc electrode) is called the anode, and the electrode in which reduction occurs (copper electrode) is called the cathode. This configuration of zinc and copper electrodes and electrolytes is called the Daniell cell (after the British chemist J.F. Daniell). In the Daniell cell, the oxidation and reduction half-reactions take place in the electrodes. The net reaction is identical to the one that happens when both metals are directly in contact:

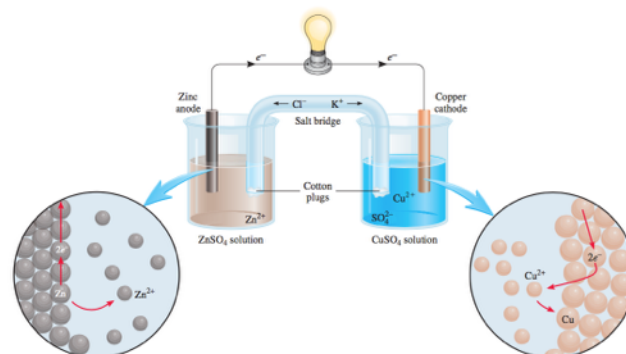
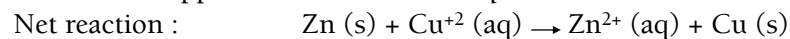
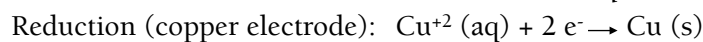
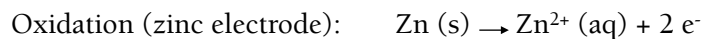


Fig 2. A galvanic cell [4]

The cathode and anode containers must be electrically neutral, however, as zinc is oxidized the anodic solution is positively charged by the Zn^{+2} ions formed. On the other side, as the copper ions are reduced to copper, the surrounding solution starts to negatively charge. This will eventually stop the electron flux. To avoid it, a salt bridge is needed: an inverted U-shaped tube that contains a conducting solution like KCl or NaCl (aq). Its ends are closed with porous stoppers. When the cell is working, the Cl^- ions move towards the side where the Zn^{+2} ions are formed, and the K^+ ions move towards the side where Cu^{+2} ions are consumed.

In the galvanic cell, the bigger the electric current is, the more quantity of Zn corrodes. The quantitative relationship of this process was first announced at the beginning of the 20th century by Michael Faraday in the following two laws:

1. The quantity of substance deposited or detached in an electrode is directly proportional to the quantity of electricity that has circulated through the dissolution.
2. For the same quantity of electricity, the quantity of substance deposited or detached is directly proportional to the equivalent weight of the substance.

For one equivalent to be deposited (or detached), it must circulate one mol of electrons (96500 C approx.) The electromotive force of a cell (*emf*) measures the potential difference between the two electrodes and hence it can be expressed as:

$$E_{cell} = E_{cathode} - E_{anode} - I \cdot r_{inner}$$

Where r_{inner} is the internal resistance of the wire and the electrodes and their value can be approximated to zero. If the electrode potentials were known, it would be relatively easy to determine the *emf* of the cell, but it is nevertheless impossible to measure it, as only potential differences can be measured. Therefore a reference electrode and the zero potential value is arbitrarily assigned to it. By international agreement, this standard electrode is the standard hydrogen electrode and it consists in a platinized platinum sheet surrounded by gaseous bubbled hydrogen at 1 atm and 25°C through a 1 M HCl solution. The standard potential assigned is 0.00 V.

The standard hydrogen electrode can be used to measure the potentials of other electrodes: the standard potential of the cell (E°) that forms with the standard hydrogen electrode. In a spontaneous reaction, the E° must be positive, in other case, the spontaneous reaction will be the contrary. The standard reduction potential of some half-reactions can be arranged in a table. These values show the reductive power of the species that contain, i.e.; their capability to accept electrons.

Half-Reaction	$E^\circ(\text{V})$
$\text{F}_2(\text{g}) + 2\text{e}^- \longrightarrow 2\text{F}^-(\text{aq})$	+2.87
$\text{O}_3(\text{g}) + 2\text{H}^+(\text{aq}) + 2\text{e}^- \longrightarrow \text{O}_2(\text{g}) + \text{H}_2\text{O}$	+2.07
$\text{Co}^{3+}(\text{aq}) + \text{e}^- \longrightarrow \text{Co}^{2+}(\text{aq})$	+1.82
$\text{H}_2\text{O}_2(\text{aq}) + 2\text{H}^+(\text{aq}) + 2\text{e}^- \longrightarrow 2\text{H}_2\text{O}$	+1.77
$\text{PbO}_2(\text{s}) + 4\text{H}^+(\text{aq}) + \text{SO}_4^{2-}(\text{aq}) + 2\text{e}^- \longrightarrow \text{PbSO}_4(\text{s}) + 2\text{H}_2\text{O}$	+1.70
$\text{Ce}^{4+}(\text{aq}) + \text{e}^- \longrightarrow \text{Ce}^{3+}(\text{aq})$	+1.61
$\text{MnO}_4^-(\text{aq}) + 8\text{H}^+(\text{aq}) + 5\text{e}^- \longrightarrow \text{Mn}^{2+}(\text{aq}) + 4\text{H}_2\text{O}$	+1.51
$\text{Au}^{3+}(\text{aq}) + 3\text{e}^- \longrightarrow \text{Au}(\text{s})$	+1.50
$\text{Cl}_2(\text{g}) + 2\text{e}^- \longrightarrow 2\text{Cl}^-(\text{aq})$	+1.36
$\text{Cr}_2\text{O}_7^{2-}(\text{aq}) + 14\text{H}^+(\text{aq}) + 6\text{e}^- \longrightarrow 2\text{Cr}^{3+}(\text{aq}) + 7\text{H}_2\text{O}$	+1.33
$\text{MnO}_2(\text{s}) + 4\text{H}^+(\text{aq}) + 2\text{e}^- \longrightarrow \text{Mn}^{2+}(\text{aq}) + 2\text{H}_2\text{O}$	+1.23
$\text{O}_2(\text{g}) + 4\text{H}^+(\text{aq}) + 4\text{e}^- \longrightarrow 2\text{H}_2\text{O}$	+1.23
$\text{Br}_2(\text{l}) + 2\text{e}^- \longrightarrow 2\text{Br}^-(\text{aq})$	+1.07
$\text{NO}_3^-(\text{aq}) + 4\text{H}^+(\text{aq}) + 3\text{e}^- \longrightarrow \text{NO}(\text{g}) + 2\text{H}_2\text{O}$	+0.96
$2\text{Hg}_2^{2+}(\text{aq}) + 2\text{e}^- \longrightarrow \text{Hg}_2^{2+}(\text{aq})$	+0.92
$\text{Hg}_2^{2+}(\text{aq}) + 2\text{e}^- \longrightarrow 2\text{Hg}(\text{l})$	+0.85
$\text{Ag}^+(\text{aq}) + \text{e}^- \longrightarrow \text{Ag}(\text{s})$	+0.80
$\text{Fe}^{3+}(\text{aq}) + \text{e}^- \longrightarrow \text{Fe}^{2+}(\text{aq})$	+0.77
$\text{O}_2(\text{g}) + 2\text{H}^+(\text{aq}) + 2\text{e}^- \longrightarrow \text{H}_2\text{O}_2(\text{aq})$	+0.68
$\text{MnO}_4^-(\text{aq}) + 2\text{H}_2\text{O} + 3\text{e}^- \longrightarrow \text{MnO}_2(\text{s}) + 4\text{OH}^-(\text{aq})$	+0.59
$\text{I}_2(\text{s}) + 2\text{e}^- \longrightarrow 2\text{I}^-(\text{aq})$	+0.53
$\text{O}_2(\text{g}) + 2\text{H}_2\text{O} + 4\text{e}^- \longrightarrow 4\text{OH}^-(\text{aq})$	+0.40
$\text{Cu}^{2+}(\text{aq}) + 2\text{e}^- \longrightarrow \text{Cu}(\text{s})$	+0.34
$\text{AgCl}(\text{s}) + \text{e}^- \longrightarrow \text{Ag}(\text{s}) + \text{Cl}^-(\text{aq})$	+0.22
$\text{SO}_4^{2-}(\text{aq}) + 4\text{H}^+(\text{aq}) + 2\text{e}^- \longrightarrow \text{SO}_2(\text{g}) + 2\text{H}_2\text{O}$	+0.20
$\text{Cu}^{2+}(\text{aq}) + \text{e}^- \longrightarrow \text{Cu}^+(\text{aq})$	+0.15
$\text{Sn}^{4+}(\text{aq}) + 2\text{e}^- \longrightarrow \text{Sn}^{2+}(\text{aq})$	+0.13
$2\text{H}^+(\text{aq}) + 2\text{e}^- \longrightarrow \text{H}_2(\text{g})$	0.00
$\text{Pb}^{2+}(\text{aq}) + 2\text{e}^- \longrightarrow \text{Pb}(\text{s})$	-0.13
$\text{Sn}^{2+}(\text{aq}) + 2\text{e}^- \longrightarrow \text{Sn}(\text{s})$	-0.14
$\text{Ni}^{2+}(\text{aq}) + 2\text{e}^- \longrightarrow \text{Ni}(\text{s})$	-0.25
$\text{Co}^{2+}(\text{aq}) + 2\text{e}^- \longrightarrow \text{Co}(\text{s})$	-0.28
$\text{PbSO}_4(\text{s}) + 2\text{e}^- \longrightarrow \text{Pb}(\text{s}) + \text{SO}_4^{2-}(\text{aq})$	-0.31
$\text{Cd}^{2+}(\text{aq}) + 2\text{e}^- \longrightarrow \text{Cd}(\text{s})$	-0.40
$\text{Fe}^{2+}(\text{aq}) + 2\text{e}^- \longrightarrow \text{Fe}(\text{s})$	-0.44
$\text{Cr}^{3+}(\text{aq}) + 3\text{e}^- \longrightarrow \text{Cr}(\text{s})$	-0.74
$\text{Zn}^{2+}(\text{aq}) + 2\text{e}^- \longrightarrow \text{Zn}(\text{s})$	-0.76
$2\text{H}_2\text{O} + 2\text{e}^- \longrightarrow \text{H}_2(\text{g}) + 2\text{OH}^-(\text{aq})$	-0.83
$\text{Mn}^{2+}(\text{aq}) + 2\text{e}^- \longrightarrow \text{Mn}(\text{s})$	-1.18
$\text{Al}^{3+}(\text{aq}) + 3\text{e}^- \longrightarrow \text{Al}(\text{s})$	-1.66
$\text{Be}^{2+}(\text{aq}) + 2\text{e}^- \longrightarrow \text{Be}(\text{s})$	-1.85
$\text{Mg}^{2+}(\text{aq}) + 2\text{e}^- \longrightarrow \text{Mg}(\text{s})$	-2.37
$\text{Na}^+(\text{aq}) + \text{e}^- \longrightarrow \text{Na}(\text{s})$	-2.71
$\text{Ca}^{2+}(\text{aq}) + 2\text{e}^- \longrightarrow \text{Ca}(\text{s})$	-2.87
$\text{Sr}^{2+}(\text{aq}) + 2\text{e}^- \longrightarrow \text{Sr}(\text{s})$	-2.89
$\text{Ba}^{2+}(\text{aq}) + 2\text{e}^- \longrightarrow \text{Ba}(\text{s})$	-2.90
$\text{K}^+(\text{aq}) + \text{e}^- \longrightarrow \text{K}(\text{s})$	-2.93
$\text{Li}^+(\text{aq}) + \text{e}^- \longrightarrow \text{Li}(\text{s})$	-3.05

Increasing strength as oxidizing agent

Increasing strength as reducing agent

Table 1. Standard reduction potentials [4]

These values only apply to ideal cells in ideal conditions (25°C, 1atm, 1M). If temperature or concentration are altered or alloy electrodes are used, the cell potential will change, and perhaps, the reaction direction may be reversed. If $[M_1^{n+}]$ and $[M_2^{n+}]$ are the molar ion concentrations of each solution and T the absolute temperature, according to the Nerst equation:

$$\Delta E = (E_2^0 - E_1^0) - \frac{RT}{nF} \cdot \ln \frac{[M_1^{n+}]}{[M_2^{n+}]}$$

where R is the gas constant, n is the number of electrons participating in either of the half-cell reactions, and F is the Faraday constant, 96500 C/mol, the magnitude of charge per mole ($6.022 \cdot 10^{23}$) of electrons.

The data from the Standard reduction potential table does not consider all these factors, and has a limited utility. Other factors that does not consider are the limited solubility of the metallic salts and the formation of protective layers in some metals. A more realistic arrangement is provided by the galvanic series. This represents the relative reactivities of a number of metals and commercial alloys in seawater.

	Platinum
	Gold
	Graphite
	Titanium
	Silver
	[316 Stainless steel (passive)
	[304 Stainless steel (passive)
	[Inconel (80Ni-13Cr-7Fe) (passive)
	[Nickel (passive)
	[Monel (70Ni-30Cu)
	Copper-nickel alloys
	Bronzes (Cu-Sn alloys)
	Copper
	[Brasses (Cu-Zn alloys)
	[Inconel (active)
	[Nickel (active)
	Tin
	Lead
	[316 Stainless steel (active)
	[304 Stainless steel (active)
	[Cast iron
	[Iron and steel
	Aluminum alloys
	Cadmium
	Commercially pure aluminum
	Zinc
	Magnesium and magnesium alloys

Table 2. The galvanic series [1]

Oxidation and corrosion affects most metals and alloys in a large variety of environments; they are more stable in an ionic state than as metals. Therefore, most of the metals are

present in nature as compounds (e.g. oxides, hydroxides, carbonates, silicates, sulfides, and sulfates). Gold and platinum are the two exceptions: they may exist in nature in the metallic state, since oxidation in most environments is not favorable. Since there is an electric current associated with the electrochemical corrosion, it can be also expressed in terms of its current density (i.e. the current per unit of surface area corroding), as follows:

$$r = \frac{i}{n \cdot F}$$

where i is the current density, r is the rate in mol/m², n the ionization electrons and F the faraday constant (96,500 C/mol)

1.3. Forms of corrosion

The following classification of corrosion is based on the appearance of the corroded metal. It can be identified by mere observation and is the most common classification, proposed by [1], [5] and [6] among others. Some other classification categories have been added following the criteria of [7] and [8]. The UNE-EN ISO 8044 standard also contains a detailed classification of types of corrosion [9]. The corrosion forms are: 1) *Uniform* or general attack; 2) *Galvanic corrosion*; 3) *Crevice corrosion*; 4) *Pitting*; 5) *Intergranular corrosion*; 6) *Selective leaching*, or parting; 7) *Erosion corrosion*; 8) *Stress corrosion*; 9) *Fatigue corrosion*, 10) *Cavitation damage*, 11) *Fretting corrosion*, 12) *Hydrogen embrittlement* and 13) *Corrosion by biofouling*.

Uniform attack: Is the most common way of corrosion. It is normally characterized by a chemical or electrochemical reaction that occur randomly over the surface. The metal becomes thinner, eventually causing a failure. Some examples include general rusting of steel and the tarnishing of silverware. Although it represents the most common form of corrosion, from a technical point of view is relatively easy to predict and prevent and the life of the metal can be estimated with accuracy. It can be prevented or reduced by proper materials, including coatings, inhibitors or cathodic protection, which can be used singly or in combination. Uniform attack is generally expressed in mm/year, in g/(mm²-day) or in mg/(dm²-day). It is necessary to know the density of the metal.

Galvanic corrosion: Galvanic corrosion because of the potential difference that usually exists between two metals or alloys having different compositions are electrically coupled and surrounded by an electrolyte. This is the type of corrosion that happens in a galvanic cell, as it has been previously described. The less resistant metal becomes the anode and the more resistant metal the cathode. The anodic metal will experience the corrosion, whereas the cathodic metal does not usually corrode at all. For example, steel screws corrode when in contact with brass in a marine environment; or if copper and steel tubing are joined in a domestic water heater, the steel will corrode in the vicinity of the junction [5]. The galvanic series is a good way to predict the behaviour of the metals in galvanic corrosion. It can be prevented or reduced by: coupling, if necessary, metals that are close

together in the galvanic series; maximize the anode area as much as possible; electrically insulate dissimilar metals; use cathodic protection by connecting electrically a third anodic metal.

Crevice corrosion: Crevices are usually affected by intensive, localized corrosion that occurs within them and other shielded areas of metal exposed to corrosives and between two regions of the same metal piece. The crevice must be wide enough for the electrolyte to penetrate, yet narrow enough for it to stay. Some gaskets or washers where rough or absorbent elements are involved represent critical points because its capacity to retain the electrolyte. Note that contact between metal and nonmetallic surfaces can lead to crevice corrosion also. It can be prevented or reduced by using welded butt joints instead of riveted or bolted joints, closing unions by continuous welding, using non-absorbing gaskets (such as Teflon) whenever possible, avoiding sharp corners and staining areas, inspecting and removing accumulated deposits frequently, and designing containment vessels to avoid stagnant areas and ensure complete drainage [1].

Pitting: In this form of corrosion, the attack occurs in a different speed depending on the part of the metal. In very small anodic zones a very deep attack can be produced, penetrating downward in a nearly vertical direction. That results in holes in the metal, usually of a small diameter. It is one of the most destructive form of corrosion and it causes equipment to fail because of perforation with only a small percent weight loss. It is besides usually difficult to detect, because of the quantity of the holes and they are often covered by rust. The formation of a pitting hole produces a differential aeration cell, where the bottom of the pitting tends to behave even more anodically, whereas the surface, more oxygenated, tends to behave more cathallytically.

Intergranular corrosion: For some alloys, intergranular corrosion occurs preferentially along grain boundaries, since they are usually slightly more reactive than the matrix. The intergranular zone acts as the anode, whereas the interior of the grain is the cathode. Since the two zones are very close to each other, the process usually evolves very fast. Intergranular corrosion can be also caused by impurities. This type of corrosion is especially prevalent in some stainless steels. When heated to temperatures between 500 and 800°C for sufficiently long time periods, these alloys become sensitized to intergranular attack. It is believed that this heat treatment permits the formation of small precipitate particles of chromium carbide (Cr_{23}C_6) by reaction between the chromium and carbon in the stainless steel. These particles form along the grain boundaries make this region highly susceptible to corrosion [5]. Duralumin and nickel in a hight temperature sulfur atmosphere are also cases of intergranular corrosion.

Selective leaching: In selective corrosion the attack occurs preferentially in one or more components of an alloy. The affected surface becomes porous, although it can keep its original appearance and shape, so it does not show this resistance and ductility loose. The most common case of selective corrosion is the dezincification of brass, in which zinc is selectively leached from a copper–zinc brass alloy. Dezincification can be reduced by removing the aggressiveness of the environment (removing the oxygen) or by cathodic protection.

Erosion corrosion: In those cases in which a relative movement between a fluid and the metal surface is involved, an increase in the corrosion is observed. The erosive effect of the fluid is not strictly the origin of corrosion, but it definitely encourages the corrosive attack. The reasons are that the fluid movement renews the electrolyte on the surface, sweeps the corrosion products and produces mechanical erosion. Almost every metal alloy is susceptible to erosion corrosion. It is especially harmful to alloys that passivate by forming a protective surface film; the abrasive action may erode away the film exposing the bare metal. It can be identified by surface grooves and waves that follow the flow of the liquid. Erosion corrosion is commonly found in piping, especially at bends, elbows, and abrupt changes where the fluid abruptly changes its direction and becomes turbulent. Also in propellers, turbine blades, valves, and pumps [5]. Erosion corrosion can be minimized by changing the design to eliminate fluid turbulence and impingement effects. Other materials with better resistance to erosion may also be used.

Stress corrosion: Stress corrosion cracking is produced the combined action of an applied tensile stress and a corrosive environment. This way of corrosion results on the formation of local galvanic cells as a consequence of the elastic and plastic deformations produced by external or residual stresses. Residual stresses are usually result of heat treatments or cold works. The deformations of the structure increase the anisotropy of the material, making some zones to act as an anode and others as a cathode. Sometimes these deformations produce the accumulation of impurities in the grain boundaries, or the formation of dislocations. Moreover, plastic deformation produces the cracking of the metal, that increases the corroding activity. It can be prevented by lowering the magnitude of the stress, increasing the cross-sectional area and applying the appropriate heat treatment to anneal out any residual thermal stresses. Some alloys in certain environments are particularly affected by stress corrosion: aluminium alloys in NaCl solutions; copper alloys in ammonia solutions; steel in seawater, NaOH and acid solutions; stainless steels in seawater, in MgCl₂ solutions or in water vapour that contains chlorides.

Fatigue corrosion: A material affected by alternate stresses under the critical stress will theoretically not suffer from fatigue failure, (i.e. it can perform an infinite number of cycles if $S_n < S_e$). However, in reality, in corrosive environments the metal will eventually fail even if the stress is lower than the critical stress value. Fatigue failure starts with the appearance of cracks in the surface (ratchet marks), where corrosion processes start to affect. This type of corrosion can vary from one case to another, depending on the material and the corrosive environment.

Cavitation damage: Cavitation is produced by the formation and violent implosion of vapour bubbles in the metal surface, that are capable of detach particles from the surface, producing pitting and holes. Cavitation appears in surfaces where the velocity of the fluid is high and leads to an important decrease in the local pressure, causing the vaporization of the fluid. Pumps, wheels, propellers and bends of the tubes are the most common places for cavitation to appear. Cavitation is not the direct cause of the corrosion, but it destroys the surface of the metal and contributes to the corrosion.

Fretting corrosion: This form of corrosion appears in the interface of materials in contact that have a relative movement between them. It produces pitting, holes or grooves on the contact areas. The friction between the surfaces erodes the rust and its particles act as an abrasive. This increases the corrosion and loosens the joint. It appears, for example, between the external ring of a bearing and its case, or between the interior ring and the axle, as a consequence of an incorrect assembly or because not having observed the tolerances.

Hydrogen embrittlement: Hydrogen embrittlement is a physical and chemical effect that produces a significant reduction in ductility and tensile strength of some metals, specially in low carbon steels. Atomic hydrogen penetrates into the material by interstitial diffusion through the crystal lattice. Concentrations as low as several parts per million can lead to cracking. Hydrogen embrittlement is similar to stress corrosion: a normally ductile metal experiences brittle fracture when exposed to tensile stress and a corrosive atmosphere. Hydrogen may come from the manufacturing process, intermediate processing such as welding, or it may enter the metal during its service life. Elevated temperatures in welding and heat treatment increase the effect of the hydrogen diffusion. Some metals like high-strength steels and martensitic steels are susceptible to hydrogen embrittlement. However, FCC alloys (austenitic stainless steels, and alloys of copper, aluminium, and nickel) are relatively resistant to hydrogen embrittlement.

Corrosion by biofouling: The activity of some microorganisms when they appear in the metal-environment interface can produce relevant changes in this interface and hence modify the conditions in which the corrosion processes take place. These microorganisms are usually bacteria, fungi and micro-algae, being bacteria the most important. These microorganisms can reproduce with ease and they can increase the corrosion speed up to 5 orders of magnitude bigger [8]. The main reasons of this effect are the addition of ions such as S^{2-} (sulfate-reducing bacteria) or Fe^{3+} (iron-oxidizing bacteria), modifications of the pH by the addition of small amounts of organic acids or altering the oxygen concentration in the interface.

1.4. Corrosion prevention

A few corrosion prevention techniques were cited relative to the forms of corrosion described. In this section, more general corrosion prevention techniques are presented. It is important to consider that corrosion prevention should be part of the design process and not something added as an afterthought. A correct interpretation of the environment and conditions in which the equipment will have to operate is crucial. In the following scheme the corrosion prevention and control factors are displayed in the design process:

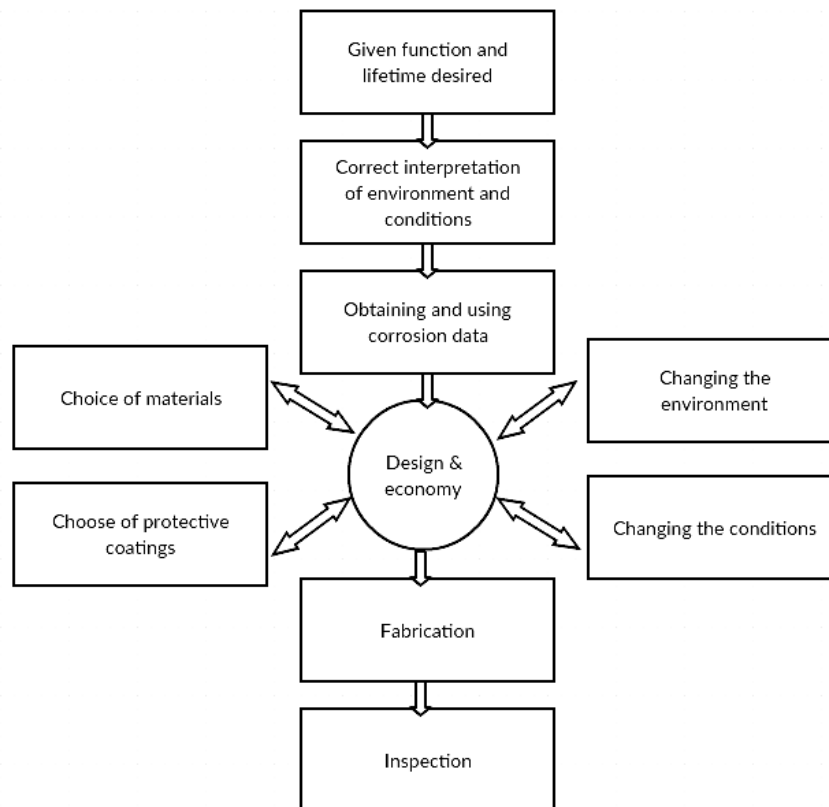


Fig 3. Design scheme showing aspects of corrosion prevention and control. [6]

Materials selection

The most common and easiest method of preventing corrosion is through the selection of the proper material for the needed service. It is therefore of major importance to have a deep knowledge on the properties of different metals and alloys, and standard corrosion references are helpful in this respect. Without going any depth in this topic, the following combinations of metal and corrosives represent the maximum amount of corrosion resistance for the least amount of money. This not represents the only material - corrosive combinations, cheaper or more resistance materials may be available [1]:

- Stainless steel - nitric acid
- Nickel and nickel alloys - caustic
- Monel - hydrofluoric acid
- Hastelloys (Chlorimets) - hot hydrochloric acid
- Lead - diluted sulfuric acid
- Aluminium - nonstaining atmospheric exposure
- Tin - distilled water
- Titanium - hot strong oxidizing solutions
- Tantalum - ultimate resistance
- Steel - concentrated sulfuric acid

Purity is also a factor that affects corrosion resistance. A pure metal is usually more resistant than another containing impurities or small amounts of other elements. Pure metals are nevertheless usually expensive and relatively weak and soft. These cases are rare, for example pure aluminium for handling hydrogen peroxide or arc-melted zirconium.

Environment and conditions

The characteristics of the environment have also great influence in corrosion. In many cases, changes in these properties can considerably reduce corrosion, but its effects vary depending on the system. Some of the factors that may be controlled are:

- **Temperature:** Lowering the temperature usually leads to a decrease in the corrosion rate. However, in some cases, the effect is the contrary, for example boiling sea water is less corrosive than hot seawater [1]. The reason is that the solubility of oxygen decreases with the increase of temperature.
- **Velocity of the fluid:** The velocity and turbulence of the fluid usually increase the corrosive attack.
- **Removing oxygen and oxidizers:** It is a very old technique and generally, the oxygen concentration decrease slows down the corrosive processes. However this may be prejudicial in the case of active-passive metals and alloys, that require oxidizers to form their protective films.
- **Concentration changes:** a direct way to reduce corrosion is to decrease the concentration of the ions in the electrolyte. Some of the devices used to decrease ion concentrations are water-treating and water-softening apparatus.

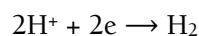
Inhibitors

The most important method to reduce corrosion is the addition of inhibiting and reducing agents to the electrolyte, specially if the electrolyte is in a closed circuit. The specific

inhibitor depends both on the alloy and on the corrosive environment: inhibitors are usually applied in metals and alloys exposed to aqueous solutions. If the corrosive environment is humid air, specially in marine environments, vapour inhibitors may be used, or if the material is exposed in a way that inhibitor properties can not be controlled, it can be applied with greases, paints or other covers. Since the effect of an inhibitor is to reduce the corrosion rate, its role in the process is essentially to decrease the corrosion current. An extensive list of corrosion inhibitors used in the oil industry can be found at [10]. Compounds with satisfactory chemical stability such SiO_2 , TiO_2 or ZrO_2 can provide powerful corrosion protection. Titanium dioxide has a very good chemical stability and heat resistance and its use jointly by silica has been successfully reported as a good corrosion inhibitor [11].

Cathodic protection

Cathodic protection consists of supplying electrons to protect the metal. It was used before the electrochemistry theories were developed, and it has been reported back to the beginning of the 19th century [1]. Electrochemical reactions follow this pattern:



The metal can be protected by a power supply or by proper galvanic coupling. In the case of the galvanic coupling, the anode is a sacrificial anode and it is consumed to protect the metal structure.

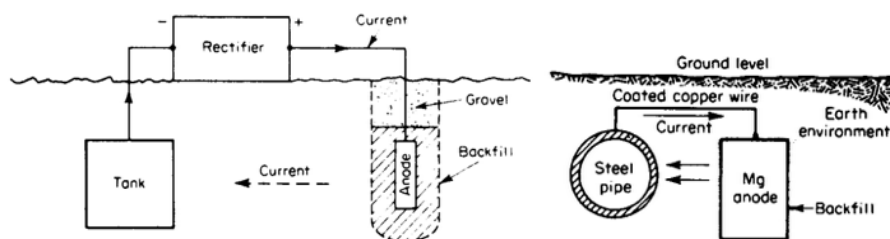


Fig 4. Cathodic protection by external power supply and by galvanic coupling. [1]

Anodic protection

Some metals such as Ti, Cr, Al, Mg, Cd, Fe and Ni among others, tend to passivate when a higher potential than the corrosion potential is applied. An increase in the corrosion potential leads to an increase in the corrosion current, which causes an increase in the corrosion rate. Anodic protection consists of the applying of external anodic currents to force the formation of a protective layer.

2. Advanced coatings for corrosion protection of aluminium alloys

2.1. Aluminium alloys

Aluminum¹ has become, after steel, the second most used metal worldwide. Its low density (2.7 g/cm³), its good corrosion resistance, its high ductility and other properties make aluminium a very interesting material for many industries. In 2014, the global production reached 54 million tonnes, and its annual growth is estimated to be around 7% [12].

The aluminium alloys classification is designated by the ANSI H35.1 standard and it consists of a four-digit nomenclature. The first digit indicates the dominant alloying element, the second one, the modification of the original alloy or the impurities limit. The last two digits indicate the minimum aluminium percentage in the 1000 series, or two identify different allows from the same series:

- **1000: 99% aluminium.** Good strength - plastic deformation relation.
- **2000: Copper.** Good mechanical properties, low corrosion resistance, low electric conductivity, ageing, difficult to weld, surface treatments.
- **3000: Manganese.** Good mechanical properties, easy machining, good corrosion resistance, hardening by deformation.
- **4000: Silicon:** Easy to cast, increase weldability, good corrosion resistance without copper.
- **5000: Magnesium:** Good mechanical properties, weldable, good corrosion resistance, hardening by deformation, surface treatments can be applied.
- **6000: Magnesium and silicon:** Good mechanical properties, good extrusion properties, very good corrosion resistance, hardening by ageing, surface treatments can be applied.
- **7000: Zinc:** Good mechanical properties, weldable if not copper is added, low corrosion resistance.
- **8000: Lithium and others.** Low density, better fatigue resistance.

¹ The IUPAC standard spelling is aluminium, even though it is also known as aluminum in the United States.

Aluminium alloys can be treated. The corresponding designation is as follows [13]:

- **F:** As fabricated. It is applied to products of a forming process in which no special control over thermal or strain hardening conditions is employed.
- **O:** Annealed. It is applied to products which have been heated to produce the lowest strength condition to improve ductility and dimensional stability.
- **H:** Strain Hardened. It is applied to products which are strengthened through cold-working. The strain hardening may be followed by supplementary thermal treatment, which produces some reduction in strength.
 - H1 – Strain Hardened Only.
 - H2 – Strain Hardened and Partially Annealed.
 - H3 – Strain Hardened and stabilized.
 - H4 – Strain Hardened and Lacquered or Painted.
- **T:** Thermally Treated. To produce stable tempers other than F, O, or H. Applies to product which has T been heat-treated, sometimes with supplementary strain-hardening, to produce a stable temper.
 - T1: Naturally aged after cooling from an elevated temperature shaping process, such as extruding.
 - T2: Cold worked after cooling from an elevated temperature shaping process and then naturally aged.
 - T3: Solution heat treated, cold worked and naturally aged.
 - T4: Solution heat treated and naturally aged.
 - T5: Artificially aged after cooling from an elevated temperature shaping process.
 - T6: Solution heat treated and artificially aged.
 - T7: Solution heat treated and stabilized (overaged).
 - T8: Solution heat treated, cold worked and artificially aged.
 - T9: Solution heat treated, artificially aged and cold worked.
 - T10: Cold worked after cooling from an elevated temperature shaping process and then artificially aged.

2.1.1. Aluminium alloy 2024

Aluminium alloy 2024 is an aluminium - copper alloy frequently used in applications that demand high mechanical characteristics such as aeronautical components, bolts or rivets. It offers a good strength - weight ratio as well as good fatigue behavior. It replaced the 2017-T4 aluminium alloy (Duralumin) in the aircraft industry. Aluminum 2024 is used in the structure of the fuselage, wings, ribs and structures where stiffness, fatigue performance and good strength are needed. It is also used in areas where elevated temperatures (up to 120°C) are present [14].

The composition of the 2024 aluminium alloy is the following [14, 15]

- Aluminum, Al : 90.7 - 94.7 %
- Chromium, Cr <= 0.10 %
- Copper, Cu: 3.8 - 4.9 %
- Iron, Fe: <= 0.50 %
- Magnesium, Mg: 1.2 - 1.8 %
- Manganese, Mn: 0.30 - 0.90 %
- Other, each: <= 0.05 %
- Other, total: <= 0.15 %
- Silicon, Si: <= 0.50 %
- Titanium, Ti: <= 0.15 %
- Zinc, Zn: <= 0.25 %

The following table shows the mechanical properties of the alloy 2024, depending on the treatment applied:

Temper	Thickness in. (mm)	Tensile Strength ksi (MPa)	Yield Strength ksi (MPa)	Elongation %
0-Sheet & plate	0.010-0.499 (0.25-12.44)	32.0 (max) (220)	14.0 (max) (96)	12
T3-Flat Sheet	0.008-0.249 (0.203-6.32)	63-64 (434-441)	42 (289)	10-15
T351-Plate*	0.250-4.000 (6.35-101.60)	64-57 (441-393)	42-41 (289-282)	12-4
T4-Coiled Sheet	0.010-0.125 (0.254-3.16)	62 (427)	40 (276)	12-15
T81-Flat Sheet	0.010-0.249 (0.254-6.32)	67 (462)	58 (400)	5
T851-Plate	0.250-1.499 (6.35-38.07)	67-66 (462-455)	58-57 (400-393)	5
*Strength Decreases as thickness increases				

Table 3. Mechanical properties of Al-2024 [14]

2.2. Main conventional techniques and their drawbacks

2.2.1. Anodizing

The anodizing process involves an electrochemical reaction that builds an aluminium oxide layer, thicker than the one that forms due to natural processes. This technique is called anodic oxidation or anodizing, because aluminium is placed in the anode of an electrolytic cell. When a DC current is applied (AC current is possible but seldom used), the oxide layer is formed and becomes a part of the material. The thickness of the barrier is determined by the temperature, the composition of the electrolyte, the current applied and the anodizing time.

The natural aluminium oxide layer has an average thickness of 0.02 μm , but after the anodizing process, this value can be raised up to 25 μm . The hardness of this layer is greater than steel. The melting point of the layer increases up to 2000°C and its isolating properties are increased; the breaking voltage is about 500-600V for a 12-15 μm layer [16]. The resulting layer consists of open pores that must be sealed in order to avoid the corrosion process. The process is therefore ended by the pore sealing. The oxide layer can be also easily colored before the sealing. The electrolyte can contain various acids, but H_2SO_4 is widely used. Corrosion resistance is limited by the presence of impurities or alloying elements, specially copper compounds. Intermetallic Al-Cu phases can solve during the process resulting on a decrease of the thickness [17]. The following figure shows the surface of anodized aluminium:

2.2.2. Chrome plating

Since the beginning of the 20th century, hexavalent chromium derivatives have been used to prevent corrosion and to improve the adherence of further coatings on zinc, magnesium, steel and aluminium alloys. Chromium (VI) or hexavalent chromium is one of the most stable oxidation state of chromium. It very seldom occurs in nature and most hexavalent chromium compounds are manufactured products. Chromates are salts that contain hexavalent chromium and have the ability to provide excellent corrosion resistance even when the surface is scratched or damaged. They dilute into the corrosive media and migrate to the bare metal surface, forming compounds that avoid corrosion.

The chrome plating process takes place usually in acid media; solutions contain chromic acid, chromates or dichromates, with a pH value around 2. On the metal surface some anodic and cathodic areas initially appear, where dissolution of the metal and hydrogen formation respectively occurs. Then, the hexavalent chromium Cr^{6+} , a strong oxidizing agent, it is reduced to trivalent chromium Cr^{3+} . In the cathodic areas where H_2 is formed, the pH increases and favours the chromate precipitation on the surface of the metal.

However, in spite of their excellent anticorrosion properties, the production, transportation, stocking, and application of hexavalent chromium are considered a very

high risk activities. It has been proved with «no need for further information and/or testing» [18] that these compounds are extremely dangerous for the environment and the ecosystems, and mortal diseases such as lung cancer or liver and kidney failure are likely to be caused by its exposure [19].

Consequently, the use of hexavalent chromium, (alongside with the use of lead, mercury and cadmium) was banned in 2006 by the European Union in the automotive and electronic industries and the development of safer alternatives is one of the main objectives of the industry.

2.3. Sol-gel coatings

Smart coatings are those that are able to respond to the environmental stimuli [20], and they are designed to fulfill specific requirements of both conventional and hi-tech demands. In the recent times, surface functionalization is one of the most developing fields, and embraces a broad panoply of techniques such as Layer-by-layer assembly or ceramic coatings obtained by sol-gel process.

Ceramic and glass coatings have been widely described in materials science and surfaces science literature [21]. A glass can be defined as an amorphous compound obtained by the melted combination of siliceous and alkali carbonates. However, since the last century, new synthetic routes have been developed to allow the preparation of glassy materials without melting. The sol-gel process is one of these chemical synthesis method. This process was first discovered in 1842, when French chemist, J.J. Ebelmen reported the synthesis of uranium oxide by heating the hydroxide[22], but the aging and heating process last almost a year to avoid cracking which reduced its applications. In the 1950s, R. Roy and other scientist changed the traditional sol-gel process into the synthesis of new ceramic oxides, making the sol-gel silicate powders quite popular. In 1971, the production process involving the hydrolysis of tetraethoxysilane (TEOS) in the presence of cationic surfactants was patented. Since then, sol-gel technology has attracted the attention in the fields of ceramics, polymer chemistry, organic and inorganic chemistry, physics [11].

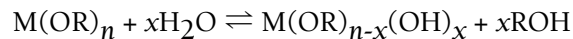
Sol-gel coatings have important advantages over conventional processes [23]:

- The temperature at which the sol-gel occurs is generally low, close to room temperature. Thus thermal volatilization and degradation of entrapped species, such as organic inhibitors, is minimized.
- Sol-gel allows to cast coatings in complex shapes, since liquid precursors are used. It also allows to produce thin films without the need for machining or melting.
- The sol-gel is considered a “green” coating technology: It uses compounds that do not introduce impurities into the end product as initial substances, this method is waste-free and excludes the stage of washing.

2.3.1. Sol-gel chemical principles

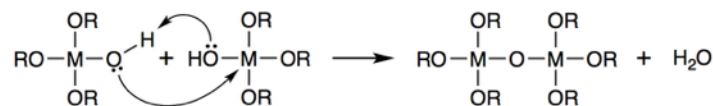
The sol-gel synthesis can be obtained from metallo-organic compounds such as alkoxides used as precursors. Alkoxides with a $M(OR)_n$ structure, where M is a metal or a metalloid and R is an alkyl group ($R = CH_3, C_2H_5, \dots$). For example, tetraethylorthosilicate (TEOS), $Si(OC_2H_5)_4$, is commonly used in the sol-gel synthesis of silica and glasses. Such chemicals are dispersed in a solvent (usually organic, ethyl alcohol) and react in an pH controlled medium, according to the following steps [24],[25]:

- Hydrolysis of the alkoxide: It is initiated by the addition of water to the silane solution under acidic, neutral or basic conditions. During the hydrolysis reaction a water molecule replaces the alkoxi (nOR) group by hydroxyl (nOH). As a result of the hydrolysis of the silicon alkoxide precursor, hydroxylated product (silanol groups) and the corresponding alcohol are generated. The reactive bond $M-OH$, which is necessary for the continuation of the reaction, is formed during this step.



- This reaction is followed by the condensation between silanol groups ($SiOH$), forming siloxanic bonds ($Si-O-Si$) and generating water or alcohol molecules as secondary products. In most of the cases, the condensation process starts before the hydrolysis is complete. The condensation can be produced between an unhydroxylated alkoxide group and a hydroxyl group (alcohol condensation or alcoxolation) or between two hydroxyl groups (water condensation or oxolation), which eliminates the solvent, and making possible the formation of a colloidal mixture known as sol.

Oxolation, which corresponds to a dehydration (the leaving group is H_2O)



Alcoxolation, which corresponds to a dealcoholation (the leaving group is ROH)

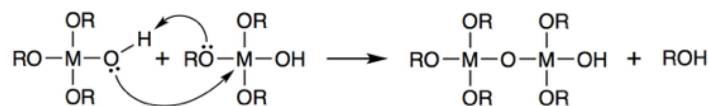


Fig 5. Sol-gel reactions [25]

When the condensation reactions are complete, each oxide ion is coordinated with four ions from the metal or metalloid, forming an homogeneous net. Depending on the chemical nature of the precursors, the final material contains one or several metal elements.

- Polycondensation between sols or additional networking, resulting in a porous and three-dimensional (3D) crosslinked network. In this situation, the viscosity of the solution is gradually increased, and as result, the sol becomes interconnected to form a rigid and porous network known as gel.

2.3.2. Sol-gel precursors

Some of the most used sol-gel precursors are shown here:

Abbreviation	Chemical name	Functional group
TEOS	Tetraethyl orthosilicate	
TMOS	Tetramethyl orthosilicate	
MTES	Methyl triethoxysilane	Methyl-
MTMS	Methyl trimethoxysilane	Methyl-
VTMS	Vinyl trimethoxysilane	Vinyl-
PTMS	Phenyl trimethoxysilane	Phenyl-
PHS	Diethylphosphonatoethyl triethoxysilane	Phosphonato-
APS	3-Aminopropyl trimethoxysilane	Amino-
AEAPS	3-(2-Aminoethyl)aminopropyl trimethoxysilane	Amino-
GPTMS	3-Glycidoxypropyl trimethoxysilane	Glycido-
MAPTS	γ -Methacryloxypropyl trimethoxysilane	Methacryloxy-
MPTMS	γ -Mercaptopropyl trimethoxysilane	Mercapto-
BTSTS	Bis-[3-(triethoxysilyl)-propyl]tetrasulfide	Sulfide-

Table 4. Some of the most commonly used precursors for sol-gel coatings [11]

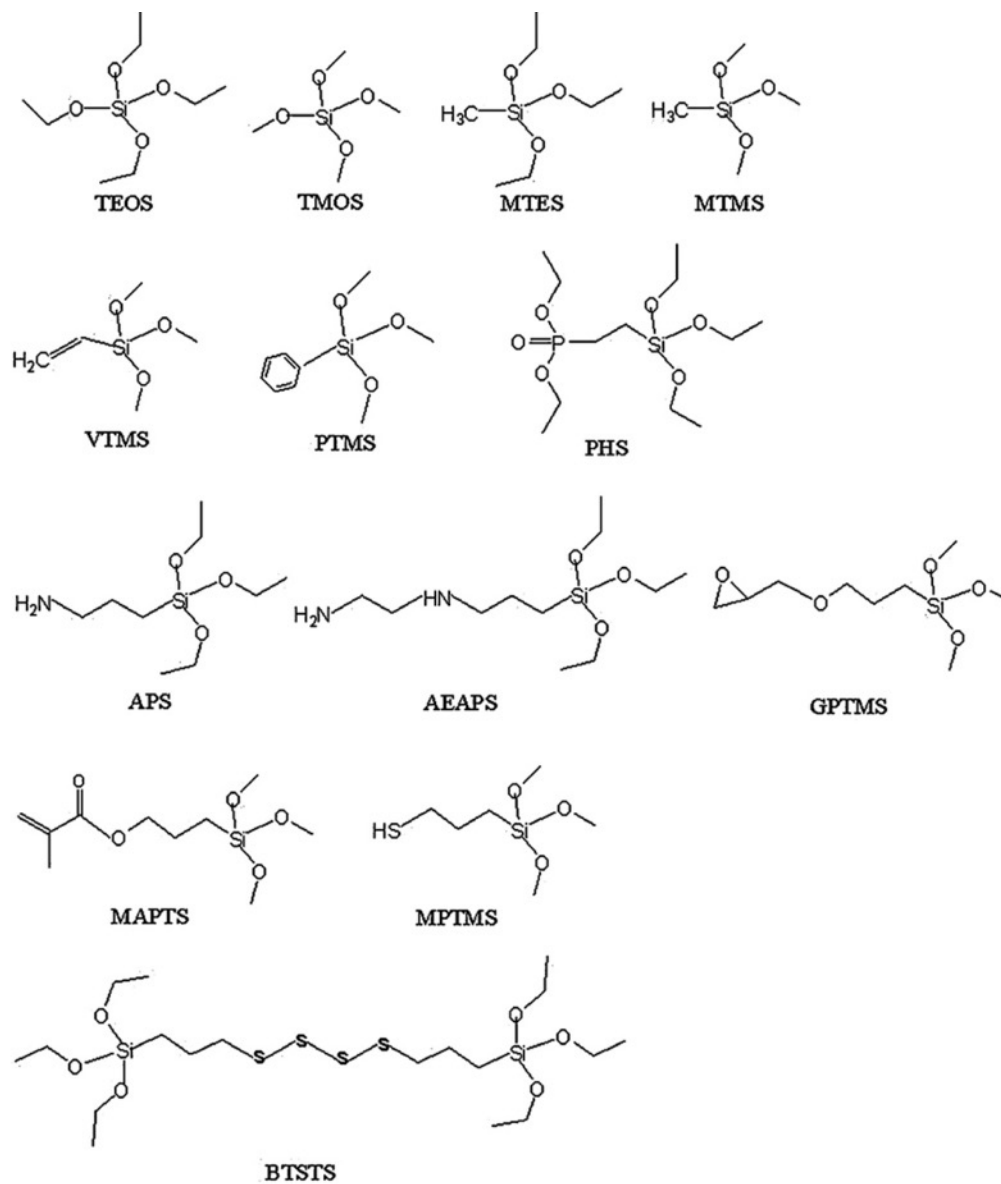


Fig 6. Chemical structure of some sol-gel precursors [11]

2.3.3. pH effects on sol-gel synthesis

In the pH range 2.5–4.5, gelation time decreases with increasing temperature, pH and water:TEOS molar ratio. Aging alcogels in ammonia produces mesoporous xerogels because of a cross-linking reaction that occurs in basic media. In the synthesis of xerogels in a basic medium, the first hydrolysis of the alkoxide groups is the rate limiting step. Once the first alkoxide group is hydrolyzed, the remaining groups hydrolyze fast, and small nuclei are created from fully hydrolyzed species. Alkaline media favours dissociation of silanol (surface) groups, which increases surface charge density and stabilizes colloidal suspensions. Consequently, gelation often requires the addition of electrolytes to destabilize the sol and obtain the alcogel [26]. The following figures show the corresponding hydrolysis reactions that occur in acid and alkaline media:

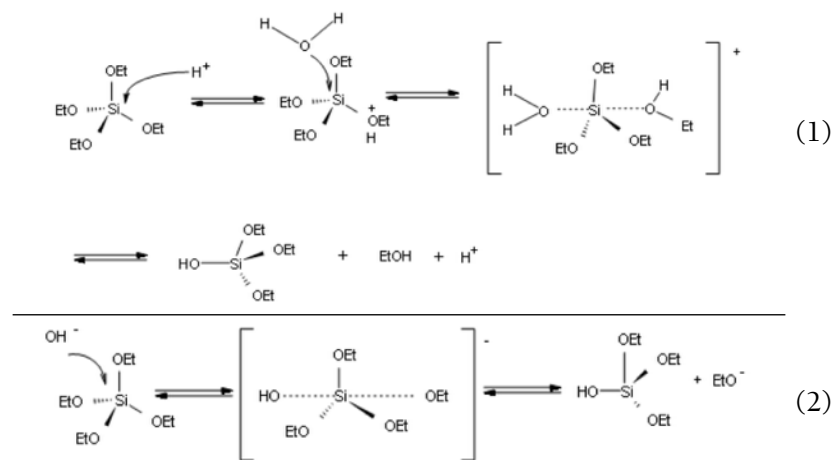


Fig 7. Hydrolysis stage reactions in an acid (1) and basic media (2) [27]

As it can be seen in the following figure, a basic medium promotes the formation of a higher cross-linked than an acid medium.

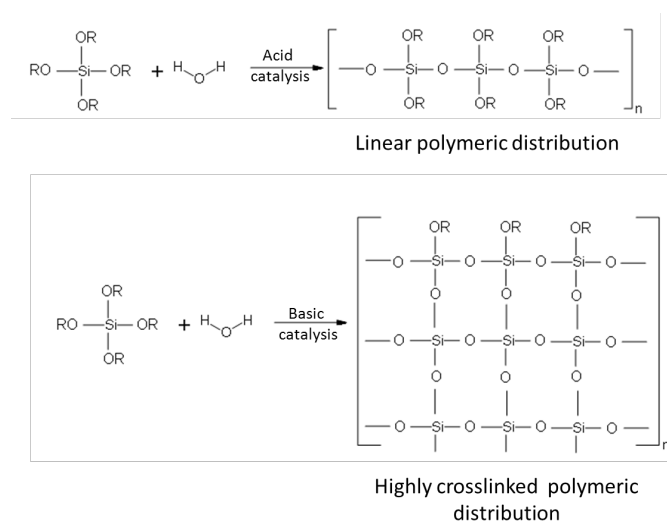


Fig 8. Hydrolysis stage reactions in an alkaline medium [27]

2.3.4. Sol-gel deposition techniques

The most common deposition procedures by which sol-gel can be applied to a metal substrate are dip-coating, spray-coating and spin-coating. Spray-coating technique has been recently developed and could be the major sol-gel coating application method in the future [11]. However, dip-coating is widely used in sol-gel depositions. Once the sol-gel precursor is prepared and aged for a specific period of time, the aluminium substrate, previously cleaned and treated, is immersed into it. Dip Coating deposition process can be divided into five steps [28]. In the continuous process, the steps are carried out directly after each other:

- Immersion: The substrate is immersed into a solution of the material to be deposited at a constant immersion rate.
- Starting: The substrate which has been dipped into the solution for a determinate period of time starts to be pulled up.
- Deposition: The film is deposited on the substrate while is pulled up. The withdrawal is carried out at a constant rate, avoiding any undesired vibration. The withdrawal speed determines the thickness of the deposited film (a higher speed produces a thicker film).
- Drainage: The excess of liquid is drained from the surface.
- Evaporation: The solvent is evaporated from the deposited liquid film, resulting on the coating. For volatile solvents, such as alcohols, the evaporation process starts during the deposition and drainage steps.

The precise control of the immersion speed, the immersion time and the withdrawal speed influences the depth and the characteristics of the resultant coating. This process is usually carried out with the help of a computer controlled robot, in which all these parameters can be easily determined. In the following image, the dip coating steps are shown. Note that this process can be repeated, and it is usually done like that. After the deposition, a drying time is needed or an ageing heat treatment can be applied, in order to reduce the humidity of the film and guarantee its stability [29].

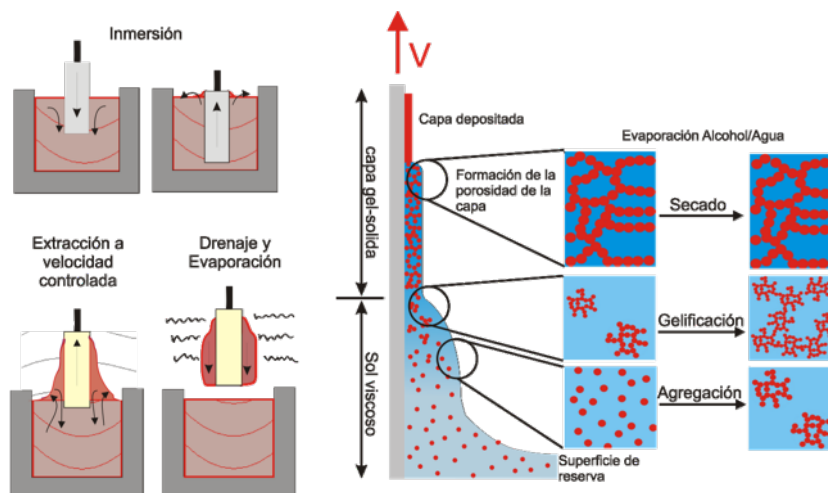


Fig 9. Dip coating process [17]

2.4. Hydrophobic coatings

Hydrophobicity phenomena are present in nature; in the leaves of plants such as *Nelumbo nucifera* (lotus), in the wings of butterflies, or in the legs of water striders. It is also a leading surface property for corrosion protection, as hydrophobic surfaces are water and aqueous electrolytes repellent, anti-icing, bio-corrosion and anti-fouling [30]. These properties can be reached by adding functional species to the coating or by modifying the composition, structure or morphology of the surface layer. Hydrophobicity is determined by the measurement of the contact angle of a water drop with the surface (WCA). Depending on the angle, three different regimes can be established:

- Hydrophilic: $10^\circ < \theta < 90^\circ$
- Hydrophobic: $90^\circ < \theta < 150^\circ$
- Superhydrophobic: $\theta > 150^\circ$

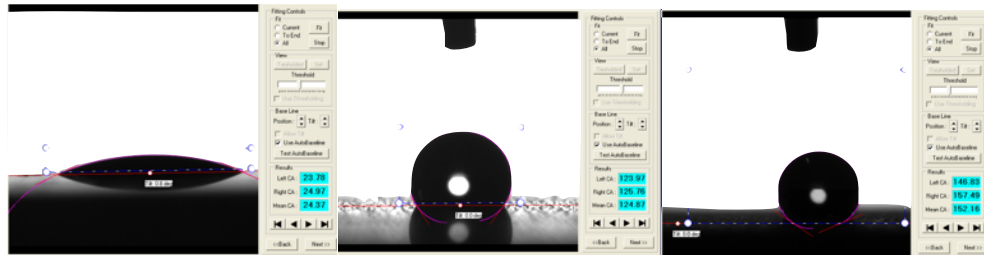


Fig 10. Hydrophilic, hydrophobic and superhydrophobic surfaces obtained by sol-gel route. Images by the author.

2.4.1. Hydrophobic surfaces theory

Atoms or molecules that are located at the surface are not able to form so many bonds with neighboring atoms than those that are in the interior, and therefore they have higher energy. This surface energy or surface tension, γ , is equal to the work required to create a unit area of the surface at constant pressure and temperature. When a drop is placed in contact with a solid, the equilibrium of the solid and liquid surfaces are established at a certain angle called the static contact angle CA, θ_0 , calculated by the Young equation [31]:

$$\cos \theta_0 = \frac{\gamma_{SA} - \gamma_{SL}}{\gamma_{LA}}$$

where γ_{SL} , γ_{SG} , γ_{LG} are the free surface energies by unit of area of, respectively, the solid-liquid, solid-gas and liquid-gas.

They can be calculated as follows:

$$\gamma = \left(\frac{\partial G}{\partial A} \right)$$

Where A is the area and G is the Gibbs free energy, obtained by the following expression:

$$G = H - TS$$

where H is the enthalpy, S the entropy and T the absolute temperature.

Wenzel model for rough surfaces: since the Young equation can not be applied to rough surfaces, Wenzel [32][33], developed a model that relates the contact angle on a rough surface, θ' to that with a flat surface θ_0 :

$$\cos \theta = r \left(\frac{\gamma_{SA} - \gamma_{SL}}{\gamma_{LA}} \right) = r \cos \theta_0$$

where r is a roughness factor, non-dimensional, and defined by the quotient between the area of a rough surface, A_{SL} , and the area of its geometric projection, A_F .

$$r = \frac{A_{SL}}{A_F}$$

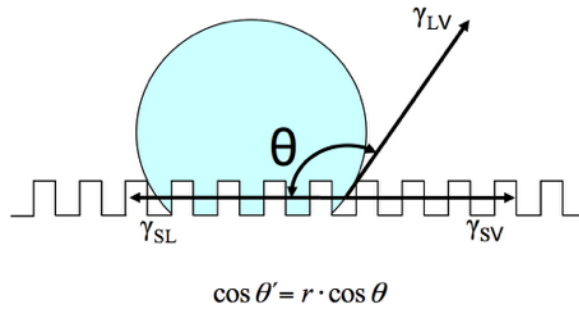


Fig 11. Liquid-solid interface according to Wenzel model [27]

Cassie-Baxter model for rough surfaces: Wenzel model is applied only for homogeneous interfaces. Therefore, another model was proposed in 1944 by Cassie and Baxter, that takes into account the air bubbles that form between the rough surface and the liquid. It consists of two fractions, each one with a fractional area and a contact angle f and θ .

$$\cos \theta' = f \cdot \cos \theta + (1-f) \cdot \cos 180^\circ = f \cdot \cos \theta + f - 1$$

where f is the fraction of the fraction of the solid surface that is in contact with the liquid.

Cassie-Baxter model is shown in the next figure:

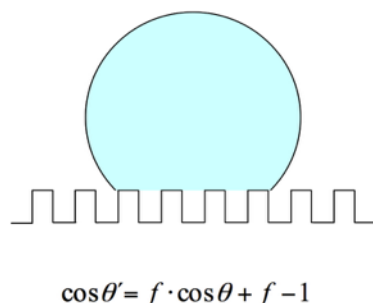


Fig 12. Liquid-solid interface according to Cassie-Baxter model [27]

2.4.2. Fabrication of hydrophobic surfaces

Hydrophobic and superhydrophobic surfaces are characterized by having a rough surface with a low surface energy. The most commonly used procedure is to make a rough surface coating and deposit on it a thin layer of a hydrophobic substance that reduces the surface energy of the materials. Sol-gel processing is a commonly used procedure to obtain hydrophobic coatings and it allows to easily modify the roughness of the resulting surface by altering the composition of the reactants.

Fluorinated coatings are a proved route to obtain hydrophobic and superhydrophobic coatings [30]. The use of fluorosilanes has been reported to produce superhydrophobic coatings as an strategy for corrosion protection [34]. The addition of these fluorinated silica particles to the coating formulations induce to high contact angles [35]. One of the most well-established fluorosilanes is the 1*H*,1*H*,2*H*,2*H*-Perfluorooctyltriethoxysilane, that can be easily added to a sol-gel coating route.

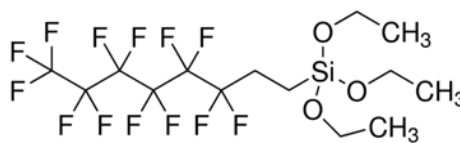


Fig 13. 1*H*,1*H*,2*H*,2*H*-Perfluorooctyltriethoxysilane [36]

2.4.3. Hydrophobic coatings for corrosion protection

Water repellent surfaces are a proved successful strategy to prevent the breaking of the oxidized layer and consequently slow down the corrosion processes. It has been described that the air that is preserved on the hydrophobic surface can avoid corrosion processes, acting like a barrier for the chloride ions from attacking the surface, for example [31]. As it is described in bibliography, hydrophobic and superhydrophobic surfaces create a

complex interface capable of retaining air [37-39] This interface decreases the contact area of the metal surface with the electrolyte and prevent ions to invade the metal.

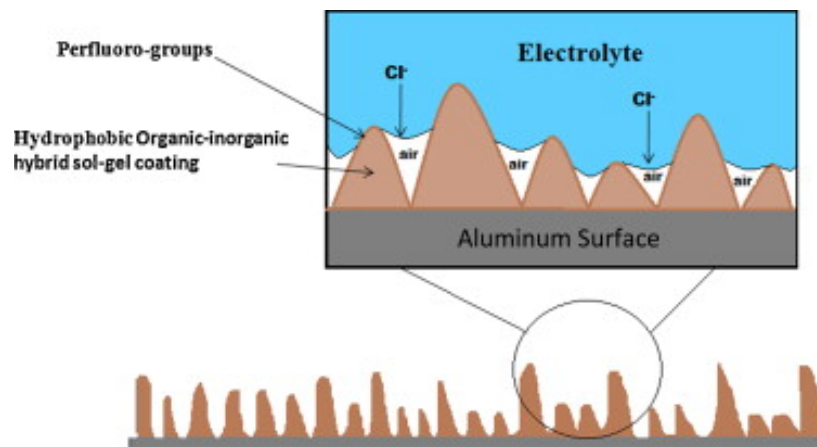


Fig 14. Superhydrophobic coating preventing the attack of chloride ions [38]

2.5. Electrospinning

Electrospinning technique was first reported by the Noble Prize John William Strutt, 3rd Baron Rayleigh, in 1897, who observed the effect that electric charge had on water jets [40]. It was studied deeper by Zeleny and patented by Formhals in 1934, who presented a setting for the fabrication of textile fibers using a voltage of 57 kV to launch cellulose acetate solved in acetone and 2-methoxyethanol [41]. The term «electrospinning» has been used since recent years as an apocope of «electrostatic spinning».

Electrospinning technique consists of the deposition of fibers on a substrate through the application of a high voltage between a polymer solution and the sample. The polymer solution, usually disposed inside a syringe with an specific needle gauge, forms a jet driven by the electrostatic potential and is deposited on the substrate, that is connected to 0 potential (ground). The thickness of the resulting fibers, unlike those obtained by conventional techniques such wet spinning, dry spinning..., can vary from the micrometer to a few nanometers [42]. The thickness depends on some variables that must be precisely controlled in order to obtain a satisfactory coating.

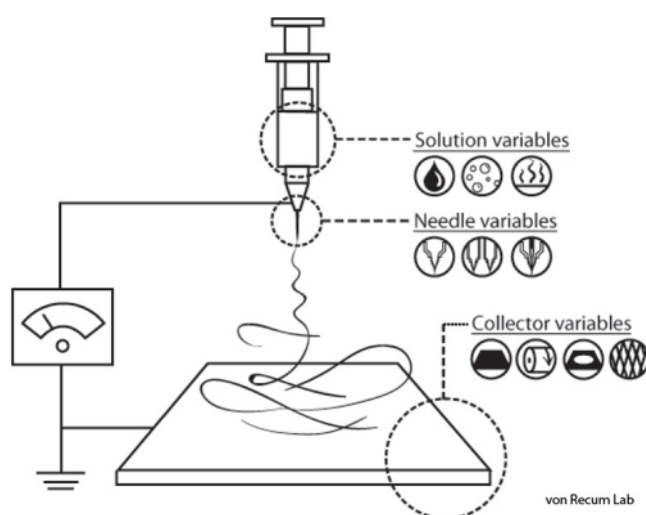


Fig 15. Electrospinning setup scheme. ©

The most important factors of the electrospinning process are the nature and viscosity of the solution, the applied voltage, the collector distance, the flow rate, the syringe gauge and the time of deposition. Rotatory collectors are also used to obtain coherent fiber directions. The usual procedure of the technique is described in bibliography [43] and an extensive list of different polymers and solvents used is also provided [44].

3. Objectives

This work has been executed within the project TRA2013-48603-C4-1-R of the Spanish Government, with the aim of developing coatings with anti-ice properties. Sol-gel and electrospinning deposition techniques have been used, since all the materials and equipment needed were available and the corresponding procedures were known by the laboratory personnel. The main objectives of this work are divided in the following steps:

- **Optimization & design**
 - Optimize the sol-gel and electrospinning techniques to obtain homogeneous coatings.
 - Optimize the hydrophobic coating technique.
 - Design of coatings combining those techniques to improve corrosion resistance of Al-2024.
- **Deposition**
 - Deposition of the coatings onto the Al-2024 substrates in order to evaluate the influence of all the parameters involved in the process.
- **Characterisation**
 - Perform corrosion tests in all the samples in order to evaluate the behaviour of each coating.

4. Methodology

4.1. Materials and equipment

4.1.1. Chemical substances

All the compounds used in this work are presented in the following section. Some of the specification sheets of the products can be found in the annexes.

- **GPTMS:** (3-Glycidyloxypropyl)trimethoxysilane. Supplied by *Sigma-Aldrich*. It is a sol-gel precursor.

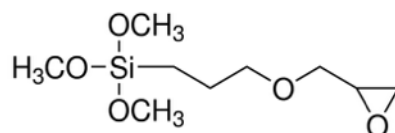


Fig 16. GPTMS [36]

- **MTEOS:** Triethoxymethylsilane. Supplied by *Sigma-Aldrich*. It is a sol-gel precursor.

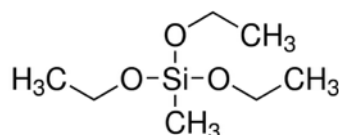


Fig 17. GPTMS [36]

- **PFAS:** 1H,1H,2H,2H-Perfluorooctyltriethoxysilane. Supplied by *Sigma-Aldrich*. It is a fluorinated sol-gel precursor.

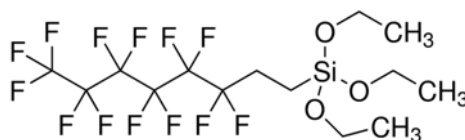


Fig 18. 1H,1H,2H,2H-Perfluorooctyltriethoxysilane [36]

- **PVA:** Poly(vinyl alcohol) . Supplied by *Sigma-Aldrich*. It is used to obtain the matrix for the electrospinning fibers.

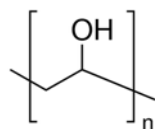


Fig 19. PVA [36]

- **PVPON:** Polyvinylpyrrolidone. Supplied by *Sigma-Aldrich*. It is used to obtain the matrix for the electrospinning fibers.

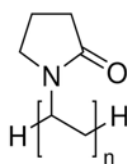


Fig 20. PVPon [36]

- **SDS:** Sodium dodecyl sulfate. Supplied by *Sigma-Aldrich*. It is used to obtain the matrix for the electrospinning fibers.

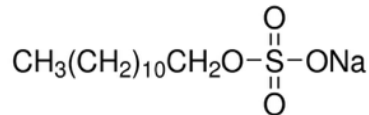


Fig 21. SDS [36]

- **TiO₂:** Titanium dioxide. Supplied by *Sigma-Aldrich*. It is used as a corrosion inhibitor. It is functionalized in NH₃.
- **Graphene oxide:** Supplied by *Graphenea*. 4 mg/mL, Water Dispersion 250 mL. It is used as a corrosion inhibitor.

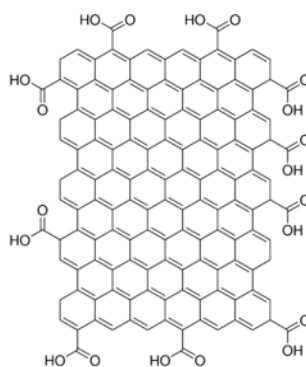


Fig 22. Graphene oxide [36]

- **Ethanol:** 99% pure $\text{CH}_3\text{CH}_2\text{OH}$. Supplied by *Panreac*. It is used in the sol-gel reactions.
- **Acetone:** dry, max 0.01% of water CH_3COCH_3 . Supplied by *Panreac*. It is used to crosslink the electrospinning fibers.
- **Hydrochloric acid:** HCl 0.1% M. Supplied by *Panreac*. It is used in the sol-gel reactions.
- **Sodium hydroxide:** NaOH 1M. Supplied by *Panreac*. It is used in the pretreatment of the surface of the aluminium samples.
- **Ultrapure water:** distilled and deionized water used in chemical reactions and to rinse the tools. The water was obtained from a *Barnstead NANOPure Diamond* ultrapure water machine, and the water obtained has a resistivity around 18-18.2 $\text{M}\Omega\cdot\text{cm}$.
- **NaCl 1M:** A solution of NaCl 1M was prepared to be used as electrolyte in the corrosion tests.

4.1.2. Equipment

In this section is presented all the equipment used for the elaboration of this work. Some of the specification sheets of the apparatus can be found in the annexes.

- **Samples:** Aluminium 2024 samples of 100 x 25 x 2.5 mm
- **ND-R Rotatory Dip Coater** (Nadetech Innovations): Programmable robot used to perform the dip coating depositions.



Fig 23. ND-R Rotatory Dip Coater [28]

- **ND-ES Lab Electrospinning Unit:** (Nadetech Innovations): Programmable robot used to perform the electrospinning depositions.



Fig 24. ND-ES Lab Electrospinning Unit [28]

- **Autolab PGSTAT204 - Compact and modular potentiostat/galvanostat** (Mettrohm autolab): compact potentiostat used to perform the electrochemical impedance spectroscopy corrosion tests. It is controlled by the *Nova* software, also distributed by Mettrohm.

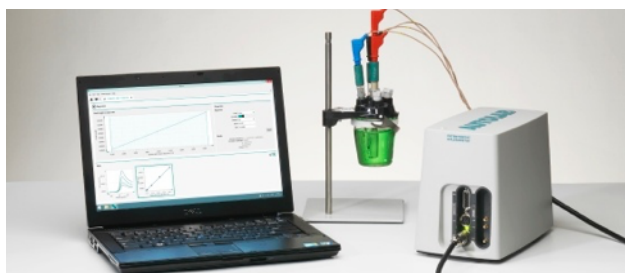


Fig 25. Autolab PGSTAT204 setup [45]

- **Voltalab PGP 201:** Potentiostat used to perform the OCP and pitting corrosion tests
- **Optical microscope Olympus BX60M with ColorView camera:** used to visualize and take pictures of the samples
- **Magnetic stirrers:** used to stir the solutions and to obtain homogeneous mixings.
- **Oven:** used to perform heat treatments and to age the coatings.
- **Optical contact angle measuring camera KSV CAM100:** used to measure the contact angles of the obtained surfaces. It consists of an adjustable plate, a needle to dose the water drops and a digital video camera connected to a computer. The corresponding software is able to automatically measure the water contact angle.

4.2. Experimental procedure

As it has been established in the objectives, the experimental design must contemplate the comparative of all the variables involved. On the bare Al-2024 substrate, different layers were applied according to:

- Sol-gel coating
- Sol-gel with TiO₂ inhibitor coating
- Sol-gel with graphene oxide inhibitor coating
- Number of dips of sol gel
- Fluorinated sol-gel layer (PFAS)
- Heat treatment of the coating
- Electrospinning fibers
- Electrospinning fibers with inhibitor

Once the coatings are deposited, the contact angle was measured to obtain the relationship between the hydrophobicity of the coating and its corrosion resistance. Subsequently pitting corrosion and electrochemical impedance spectroscopy tests were performed. Images of the coating were also taken with the microscope. The following diagram shows the overall procedure:

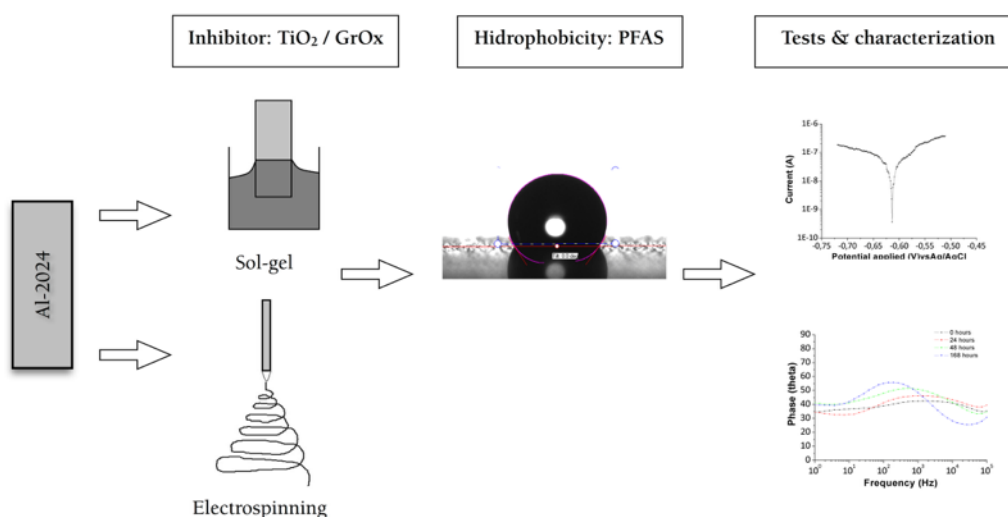


Fig 26. Overall procedure

4.2.1. Preparation of the surface of the aluminium samples

The preparation of the surface is presented in various standards: ISO 8502 provides testing for the cleanliness of surfaces, ISO 11124 establishes the requirements of the of the metallic abrasives. The main procedures are the removal of surface contamination, the removal of previous corrosion products and checking the physical condition of the surface [46].

The specific aluminium surface preparation is deeply studied in bibliography [47]. In any treatment applied, the cleanliness of the surface is a key factor in the final coating quality and durability. As it is also described, physical contamination such as lubricant residues from working operations, adherent and particles resulting from the machining may be present on the surface. The cleaning process consists of two main steps [47]:

- Solvent degreasing: physical contaminants and oily residues are removed by organic solvents. The most efficient procedure, according to the bibliography, is to first immerse the aluminium in hot solvent, followed by a cooling and a final vapor treatment to wash off oils and detritus. With no going any deeper, some of the solvents present serious problems because of their toxicity and depletion of the ozone layer.
- Alkaline cleaning: It dissolves a surface layer of the metal to remove adhered oxidation products and subsurface contamination. It is easier to attack aluminium in alkaline than in acidic solutions (view figure). Sodium carbonate, sodium (III) phosphate or sodium metasilicate are used to clean the surface. NaOH attacks the metal readily and may cause etching in its surface. Process is by immersion of the metal for a few minutes in the solution.

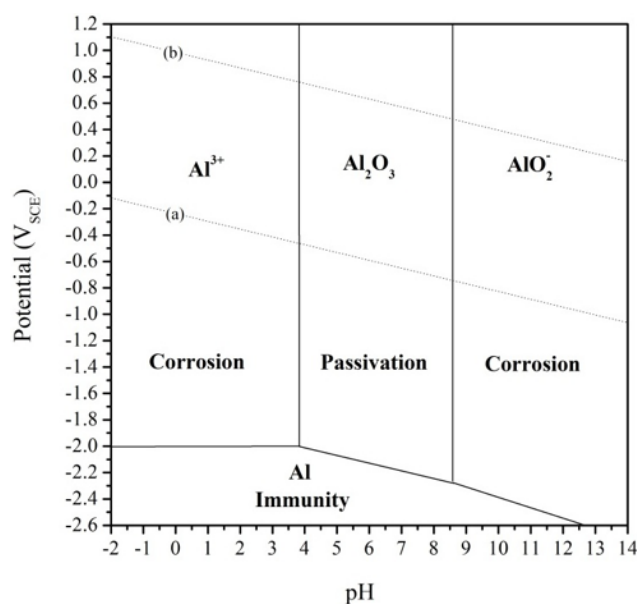


Fig 27. Pourbaix diagram for pure Al at 25°C in aqueous solution [48]

The following images were obtained by the optical microscope and show the surface of an aluminium 2024 sample before and after the NaOH treatment.

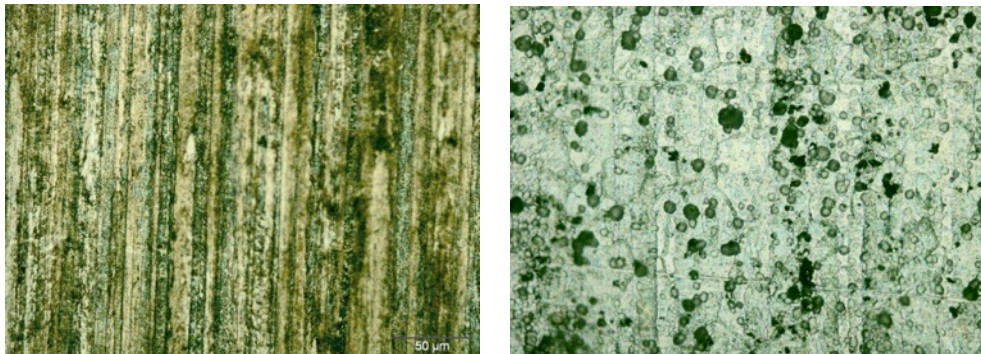


Fig 28. Al-2024 before and after the NaOH treatment. Images by the author.

4.2.2. Sol-gel depositions by dip coating

In order to take into account all the variables sixteen samples plus one control sample of Al-2024 were used. As it was found in bibliography, hybrid sol-gel systems have a major flexibility to accept additives, such as corrosion inhibitors [11]. TMOS-GPTMS hybrid matrices (1:3 mol ratio) have been proved to have a good inhibitor tolerance [49, 50]. Hybrid GPTMS-MTEOS matrices were prepared and aged and then the titanium dioxide and graphene oxide inhibitors were added in a low concentration.

To some of the samples, an additional PFAS coating was added in order to increase their hydrophobic properties. In the following table appear all the samples with their coatings and deposition data. Samples 5, 7, 13 and 15 were thermally treated at 180°C overnight to obtain a more compact and stable coating.





S.	1 st Coating	Dips	Date	2 nd Coating	Dips	Date	H.T.
0	CONTROL: Bare Al-2024						
1	GPTMS+MTEOS	1	11/apr/16				
2	GPTMS+MTEOS+Gr.Ox	1	11/apr/16				
3	GPTMS+MTEOS+TiO ₂	1	11/apr/16				
4	GPTMS+MTEOS+Gr.Ox	1	11/apr/16	PFAS	1	18/apr/16	
5	GPTMS+MTEOS+Gr.Ox	1	11/apr/16	PFAS	1	18/apr/16	
6	GPTMS+MTEOS+TiO ₂	1	11/apr/16	PFAS	1	18/apr/16	
7	GPTMS+MTEOS+TiO ₂	1	11/apr/16	PFAS	1	18/apr/16	
8	PFAS	1	15/apr/16				
9	GPTMS+MTEOS	6	11/apr/16				
10	GPTMS+MTEOS+Gr.Ox	6	11/apr/16				
11	GPTMS+MTEOS+TiO ₂	6	15/apr/16				
12	GPTMS+MTEOS+Gr.Ox	6	15/apr/16	PFAS	6	18/apr/16	
13	GPTMS+MTEOS+Gr.Ox	6	15/apr/16	PFAS	6	18/apr/16	
14	GPTMS+MTEOS+TiO ₂	6	15/apr/16	PFAS	6	19/apr/16	
15	GPTMS+MTEOS+TiO ₂	6	15/apr/16	PFAS	6	19/apr/16	
16	PFAS	6	15/apr/16				

Table 5. Summary of the sol-gel depositions obtained by dip coating

4.2.3. Electrospinning deposition

A PVA-PVPON-SDS matrix was used to deposit the electrospinning fibers. Once all the parameters were adjusted and homogeneous fibers were obtained, the corrosion inhibitor was dispersed into the matrix and deposited on the Al-2024 substrate. In order to obtain an homogeneous and stable coating, it was cross-linked both thermal and chemically. It was submerged in acetone for overnight and then dried in the oven. To obtain hydrophobic coatings, an additional PFAS coating was intended to be deposited.

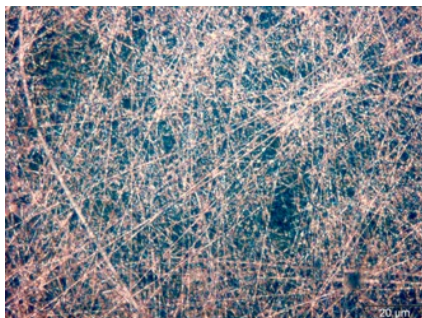


Fig 29. Electrospinning fibers with TiO₂. Optical microscope 100x

4.2.4. Water contact angle measurement

The water contact angle of all the samples was measured with the optical contact angle measuring camera. The software automatically calculates the angle that forms a water drop with the surface of the coating, in both sides of the drop. Then calculates the average and gives the measurement of the WCA.

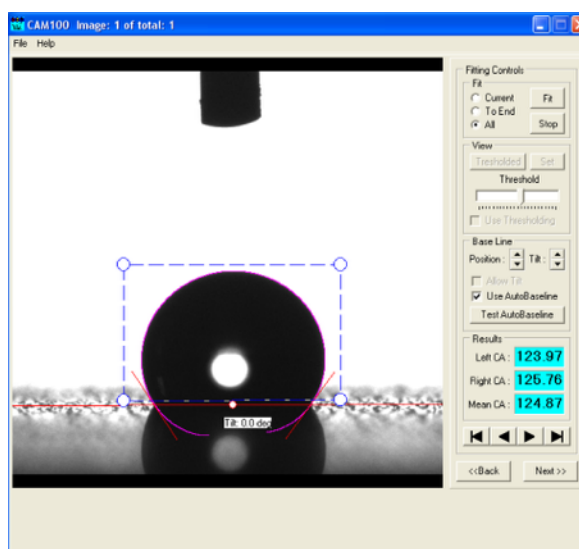


Fig 30. CAM100 software screenshot

4.2.5. Pitting corrosion tests

Open circuit potential (OCP) and pitting corrosion tests were both performed using a NaCl 1M electrolyte. The reference was an Ag/AgCl electrode and a platinum coil was used as an auxiliary electrode. The electrodes were connected to the VOLTALAB PGP201 and controlled by a computer through the corresponding software (Voltmaster 4).

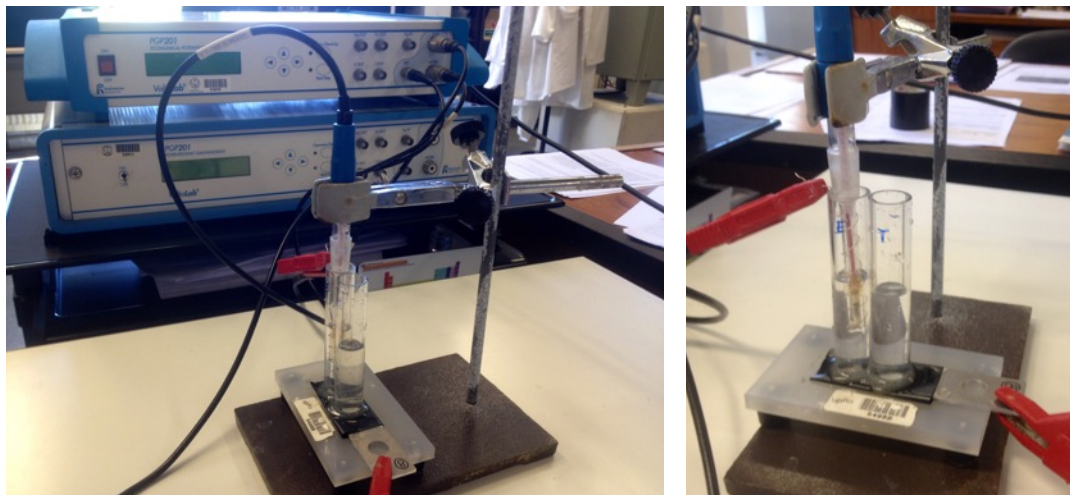


Fig 31. Voltalab setup

In open circuit potential tests, the sample was immersed in the NaCl solution for 30 minutes until the OCP between the aluminium and the reference electrode was stabilized. Then the pitting corrosion tests started. A potential was applied between the the sample and the reference electrode and the DC current was measured. When the maximum current reached the $5\text{mA}/\text{cm}^2$, the potential was programmed to decrease to its initial value. Then a *current density - potential* curve was obtained, in which the pitting potential can be easily seen. The current density remains at zero while potential increases, until pitting appears in the sample. This effect produces an increase in the current density that is detected and recorded.

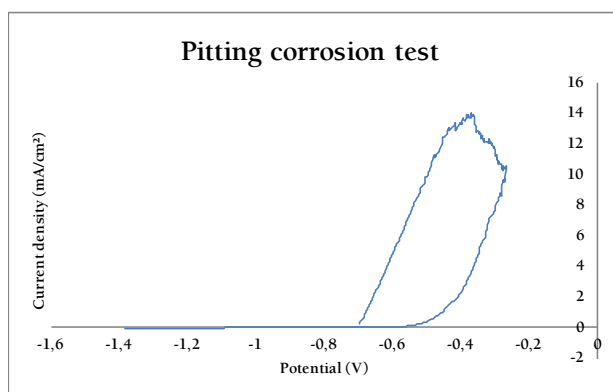


Fig 32. Pitting corrosion test result

The software is also able to calculate the Tafel curve $\log(\text{current density}) - \text{potential}$ and automatically calculates an estimated value for the corrosion rate per year.

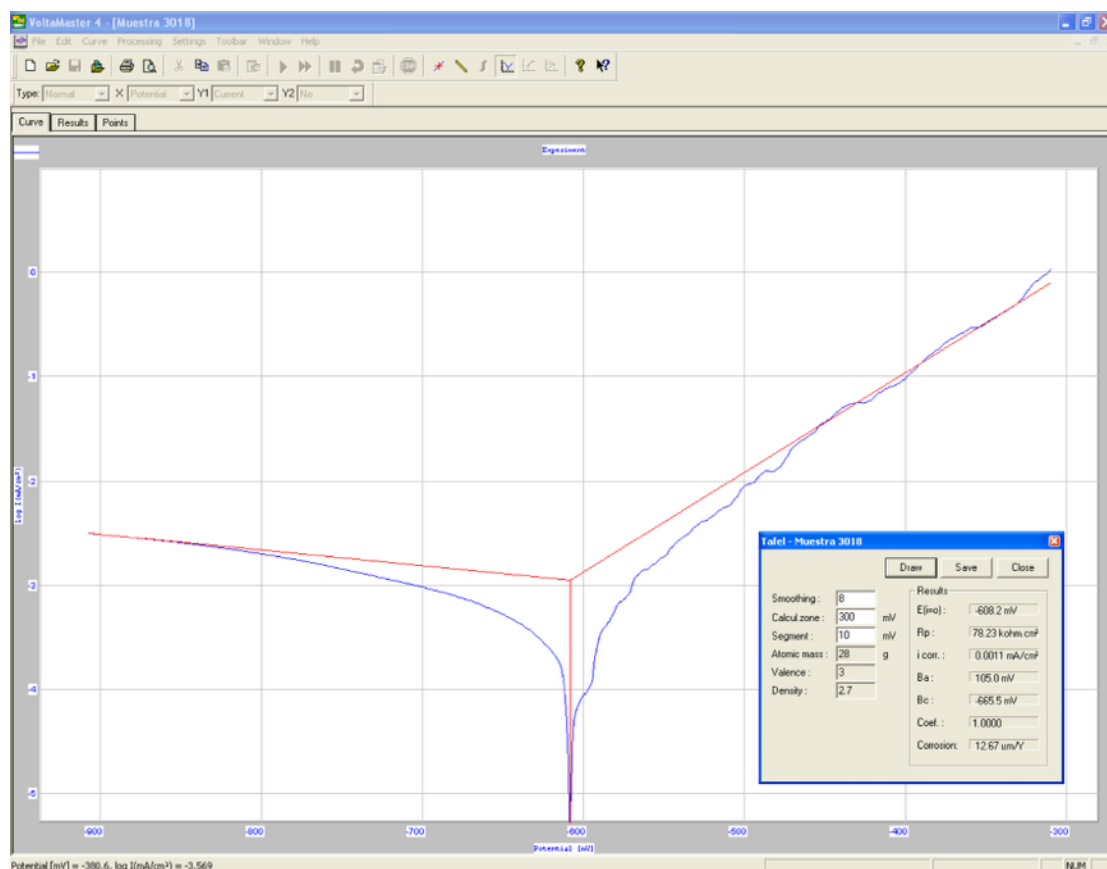


Fig 33. Tafel curve in Voltmaster 4 screenshot

4.2.6. Electrochemical impedance spectroscopy test

The electrochemical impedance spectroscopy (EIS) test consist on the application of small potential disturbances of a sinusoidal form (AC) in a wide range of frequencies. Each current response of the system to each frequency is measured and then the impedance of the system can be calculated as the quotient between the applied potential and the current response. Impedance represents the ability of a circuit to oppose to the electrical current flow, but in contrast to electrical resistance, impedance depends on the frequency of the applied stimuli and can alter the phase of the response [51].

The excitation signal is usually small enough to guarantee that the system is not polarized and the cell's response is pseudo-linear, i.e. the response to a sinusoidal excitation is a sinusoid of the same frequency although shifted in phase. Note that EIS is a non-destructive technique.

The excitation signal is of the form: $E(t) = E_o \sin(\omega t)$, and produces a response of the form $I(t) = I_o \sin(\omega t + \varphi)$. Therefore, according to Ohm's law the impedance of the system can be calculated as follows:

$$Z = \frac{E(t)}{I(t)} = \frac{E_o \sin(\omega t)}{I_o \sin(\omega t + \varphi)} = Z_o \frac{\sin(\omega t)}{\sin(\omega t + \varphi)}$$

The impedance depends on a magnitude, Z_o , and the phase shift, φ . Euler's equation allows to represent the impedance as a complex number:

$$Z(\omega) = \frac{E}{I} = Z_o \cdot e^{j\varphi} = Z_o(\cos\varphi + j\sin\varphi)$$

Where Z is composed by a real and an imaginary part. If the imaginary part is represented against the real part for different values of ω , a Nyquist plot is obtained. Moreover, Bode plots can be also obtained by representing $\log(Z)$, and the phase angle φ against $\log(\omega)$ in rad/s or in Hz.

EIS tests were carried out with a Autolab PGSTAT204 potentiostat-galvanostat and its corresponding software *Nova*. Samples were immersed in a NaCl 1M solution, a Ag/AgCl electrode was reference and a platinum coil was used as counter-electrode.

The complexity of the mathematical comprehension of the EIS results can be solved in a quantitative way by adjusting the experimental data to an equivalent electric circuit. Note that an equivalent circuit is not a real model, but an analogy. Equivalent circuits were obtained from the Bode and Nyquist plots with the help of the ZView Software. The model chosen for the circuits it's a two-mesh RC circuit, as it is proposed in bibliography for porous films on corrodible metals [17, 52-57]

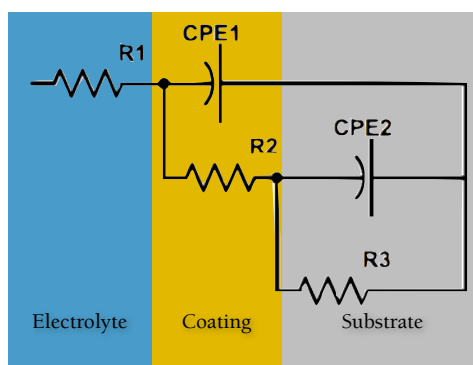


Fig 34. Proposed equivalent circuit for the coatings

Each of the components of the equivalent circuit has its analogous component in the real coating; R1 is the electrolyte resistance, CPE1 is the coating capacitance, R2 is the pore resistance, CPE2 is the double layer capacitance and R3 represents the electrochemical reactions on the metallic substrate in contact with the electrolyte. This interpretation of the EIS data is based on electrical components that represent electrochemical processes that occur in reality. Different components such as capacitors, resistors or coils can be used, but the proposed model consists of:

- **Resistances:** model the electronic/ionic conductivity and represent a charge transference.
- **Capacitors:** represent intact layers and surface interfaces, but are usually substituted by constant phase elements (CPE) that are non ideal capacitors, susceptibles to impurities, cracks... When the liquid starts to diffuse into the coating, the electrolyte enters the pores and it does not behave as an ideal capacitor any more. The relation between a CPE and an ideal capacitor is determined by a parameter, α , that can vary between 0 and 1. If $\alpha=0$, it behaves as a resistor (porous layer), if $\alpha=1$, as an ideal capacitor (compact layer). The closer to 0 the more diffusion processes are taking place.

The study of the evolution of these parameters allows to have a good notion of the real behaviour of the coating. Each of the samples were submerged in a NaCl 1M and EIS tests were performed at intervals of 1hour, 24 hours, 48 hours and 168 hours.

5. Results

In this section are presented and discussed all the results obtained. Firstly the results from the different tests are shown in section 5.1 and its relationship with corrosion resistance is then interpreted and discussed in section 5.2.

5.1. Experimental results data

5.1.1. Water contact angle measurement results

The following water contact angle values were obtained:





S.	1 st Coating	Dips	2 nd Coating	Dips	H.T.	W.C.A.
0	CONTROL: Bare Al-2024					17.14°
1	GPTMS+MTEOS	1				22.16°
2	GPTMS+MTEOS+Gr.Ox	1				24.37°
3	GPTMS+MTEOS+TiO ₂	1				101.77°
4	GPTMS+MTEOS+Gr.Ox	1	PFAS	1		95.31°
5	GPTMS+MTEOS+Gr.Ox	1	PFAS	1		103.6°
6	GPTMS+MTEOS+TiO ₂	1	PFAS	1		87.96°
7	GPTMS+MTEOS+TiO ₂	1	PFAS	1		98.44°
8	PFAS	1				87.35°
9	GPTMS+MTEOS	6				17.76°
10	GPTMS+MTEOS+Gr.Ox	6				36.24°
11	GPTMS+MTEOS+TiO ₂	6				94.52°
12	GPTMS+MTEOS+Gr.Ox	6	PFAS	6		107.23°
13	GPTMS+MTEOS+Gr.Ox	6	PFAS	6		124.87°
14	GPTMS+MTEOS+TiO ₂	6	PFAS	6		108.09°
15	GPTMS+MTEOS+TiO ₂	6	PFAS	6		120.04°
16	PFAS	6				107.44°

Table 6: Water contact angle results

Note that TiO₂ has a better hydrophobic behaviour than graphene oxide. Nevertheless, once PFAS is added, the values are more or less equal. Also those with six dips have a higher contact angle. This is shown in the following chart:

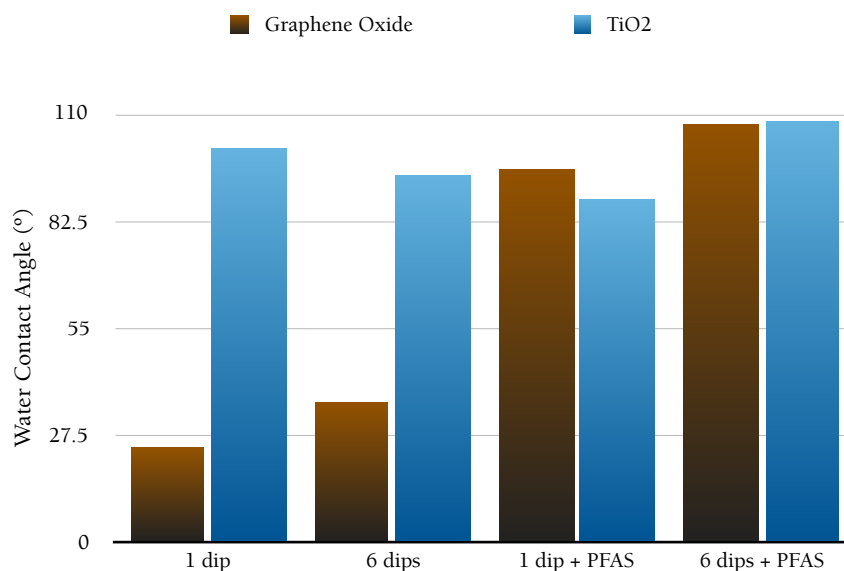


Fig 35. Dips and PFAS WCA comparison

A heat treatment helps to completely dry the coating and to force the formation of hydrogen bonds. The resulting coating is more stable and water-repellent, as it is shown in the following chart. Note that the heat treatment increases the WCA in almost 10°.

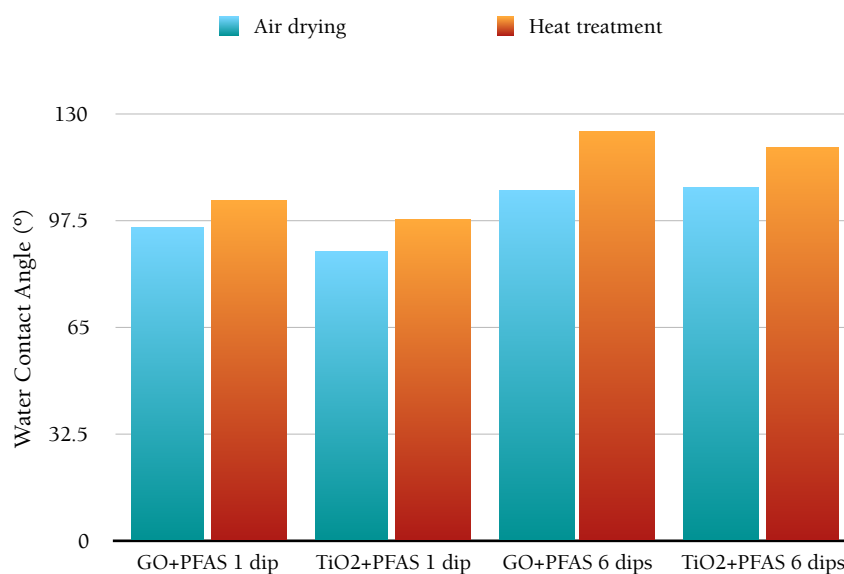


Fig 36. Dips and PFAS WCA comparison

5.1.2. Pitting corrosion test results

The following table shows the pitting corrosion voltage for each of the samples. As it can be seen, the potential of the one dip samples and the control sample is considerably lower (negative) than the potential of the 6 dips samples.





S.	1 st Coating	Dips	2 nd Coating	Dips	H.T.	E _{pitting} (mV)
0	CONTROL: Bare Al-2024					-570
1	GPTMS+MTEOS	1				-540
2	GPTMS+MTEOS+Gr.Ox	1				-520
3	GPTMS+MTEOS+TiO ₂	1				-420
4	GPTMS+MTEOS+Gr.Ox	1	PFAS	1		-420
5	GPTMS+MTEOS+Gr.Ox	1	PFAS	1		-420
6	GPTMS+MTEOS+TiO ₂	1	PFAS	1		-500
7	GPTMS+MTEOS+TiO ₂	1	PFAS	1		-540
8	PFAS	1				-500
9	GPTMS+MTEOS	6				-520
10	GPTMS+MTEOS+Gr.Ox	6				-330
11	GPTMS+MTEOS+TiO ₂	6				-300
12	GPTMS+MTEOS+Gr.Ox	6	PFAS	6		-500
13	GPTMS+MTEOS+Gr.Ox	6	PFAS	6		-280
14	GPTMS+MTEOS+TiO ₂	6	PFAS	6		-450
15	GPTMS+MTEOS+TiO ₂	6	PFAS	6		-400
16	PFAS	6				-420

Table 7: Pitting corrosion tests results

Once the pitting corrosion tests have been performed, the pitting marks can be easily identified on the surface of the aluminium sample. An image was taken under the optical microscope and the pitting area was measured with the help of a software obtaining a value of $105911.3 \mu\text{m}^2$.

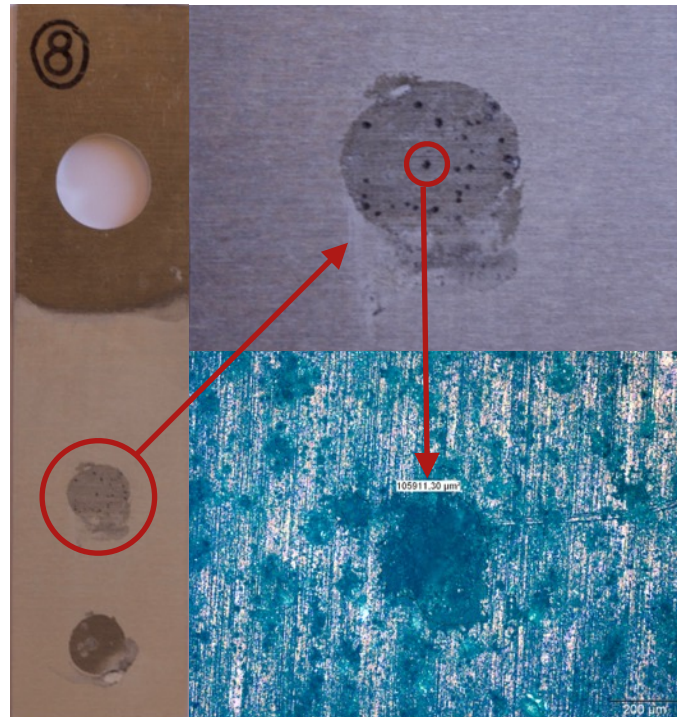


Fig 37. Pitting corrosion marks on the aluminium sample. General and microscope view. Pitting mark area: $105911.3 \mu\text{m}^2$.

5.1.3. Electrochemical impedance spectroscopy test results

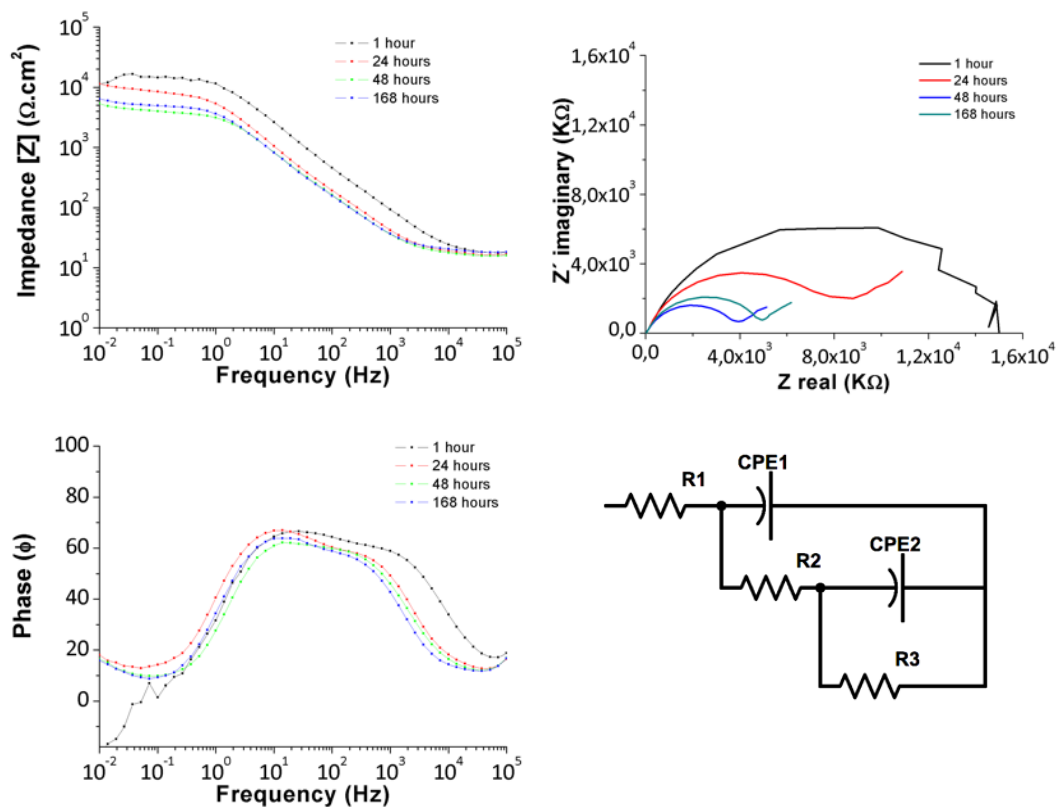
In the following pages, the results of the EIS tests are presented. The Bode diagrams of impedance and phase are shown, together with the Nyquist plot for each of the samples and each of the time intervals (1hour, 24 hours, 48 hours and 168 hours). The samples were submerged in a NaCl 1M solution for a week and during that time, EIS tests were performed.

The Bode and Nyquist plots were post processed with the ZView software, and the values were fitted to an equivalent electrical circuit. The values of the parameters are displayed as follows:

Bode impedance	Nyquist
Bode phase	Equivalent circuit
Electrical circuit parameters	

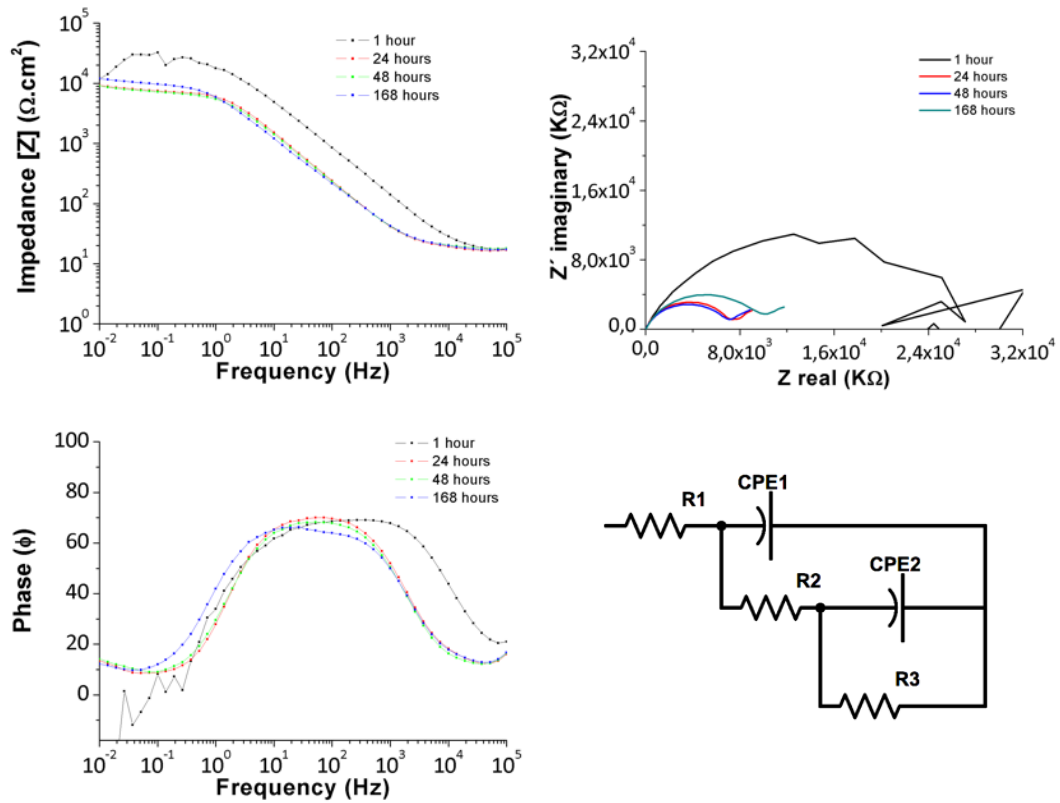
Fig 38. Electrochemical impedance spectroscopy test results display

Sample 1: GPTMS+MTEOS, 1 dip



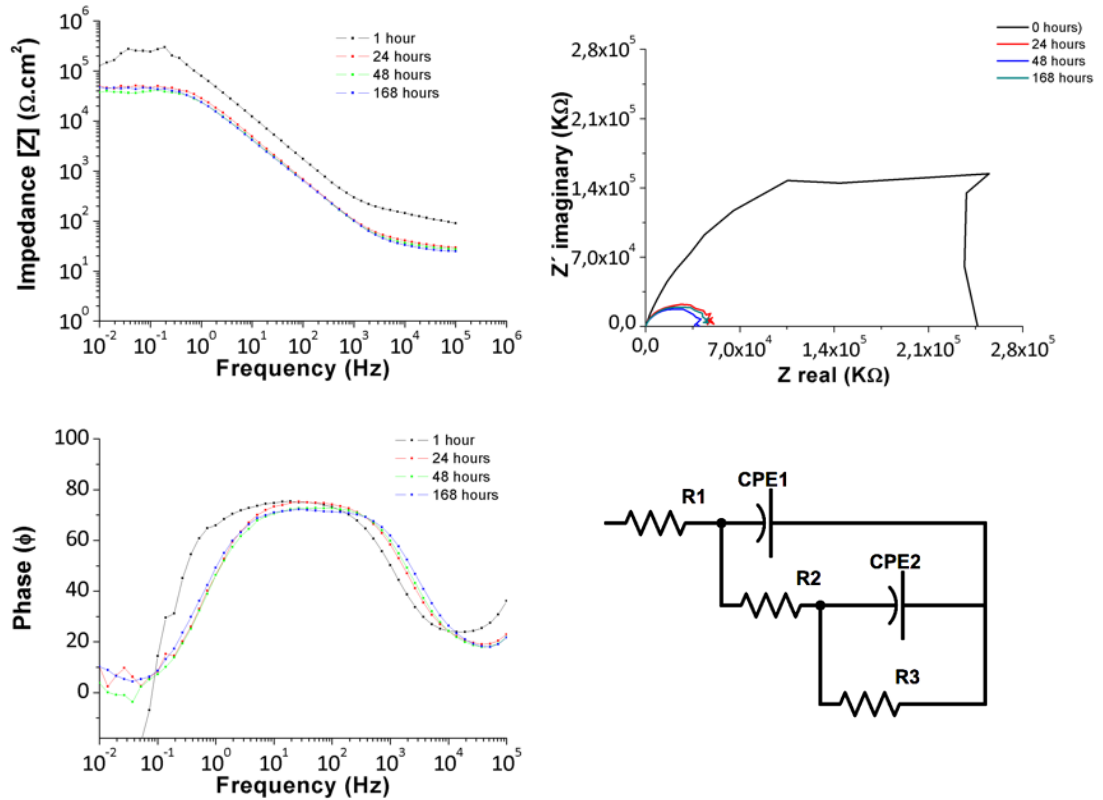
	R_1 ($\Omega \cdot \text{cm}^2$)	CPE_1 (F/cm)	α_1	R_2 ($\Omega \cdot \text{cm}^2$)	CPE_2 (F/cm)	α_2	R_3 ($\Omega \cdot \text{cm}^2$)
1h	7.018	2.05E-05	0.81161	381.5	5.23E-06	0.91703	6406
24h	15.91	2.47E-05	0.80416	551.3	6.00E-06	0.9	3.5637
48h	15.29	3.36E-05	0.79301	632.3	7.26E-06	0.89	6.839
168h	7.973	6.65E-05	0.81385	202.7	2.18E-05	0.88	3.7739

Sample 2: GPTMS+MTEOS+Graphene Oxide, 1 dip



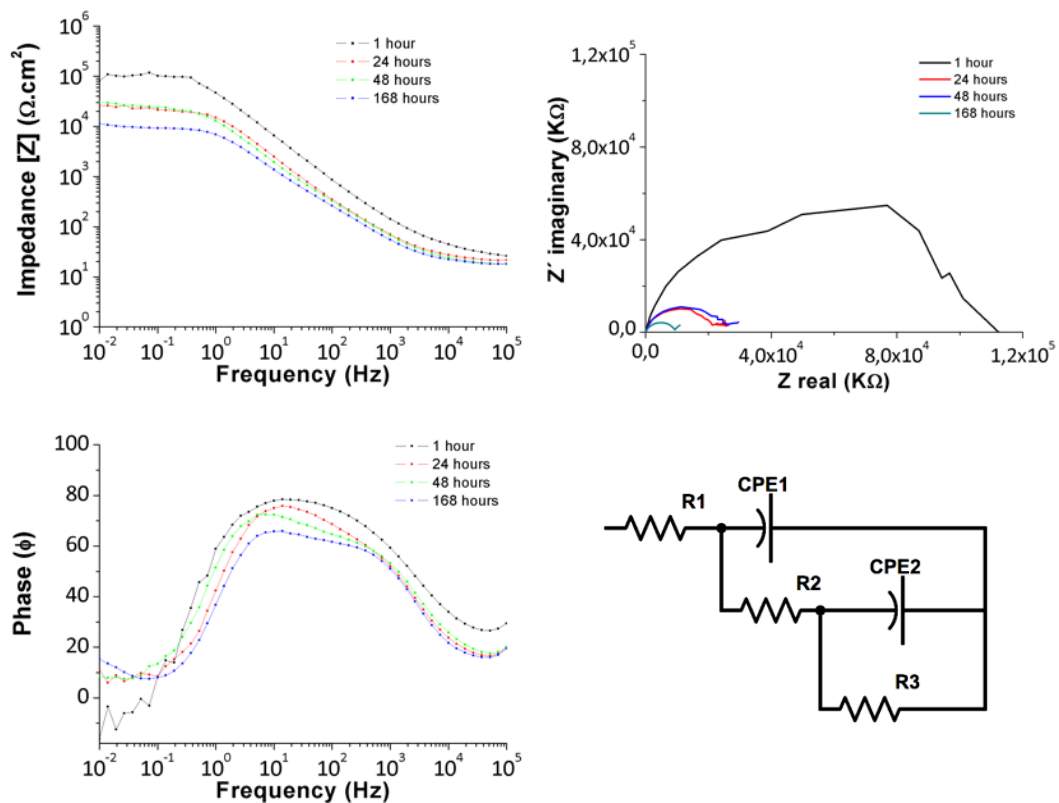
	R1 ($\Omega \cdot \text{cm}^2$)	CPE1 (F/cm)	α_1	R2 ($\Omega \cdot \text{cm}^2$)	CPE2 (F/cm)	α_2	R3 ($\Omega \cdot \text{cm}^2$)
1h	3.789	5.73E-06	0.74384	4.195	9.99E-06	0.82239	12085
24h	10.14	1.60E-06	0.83774	8.716	1.70E-05	0.84336	7790
48h	1.24E-06	3.79E-07	0.79763	18.78	2.13E-05	0.82594	7548
168h	4.28E-07	8.83E-07	0.79792	7.841	6.59E-05	0.7899	4769

Sample 3: GPTMS+MTEOS+TiO₂, 1 dip



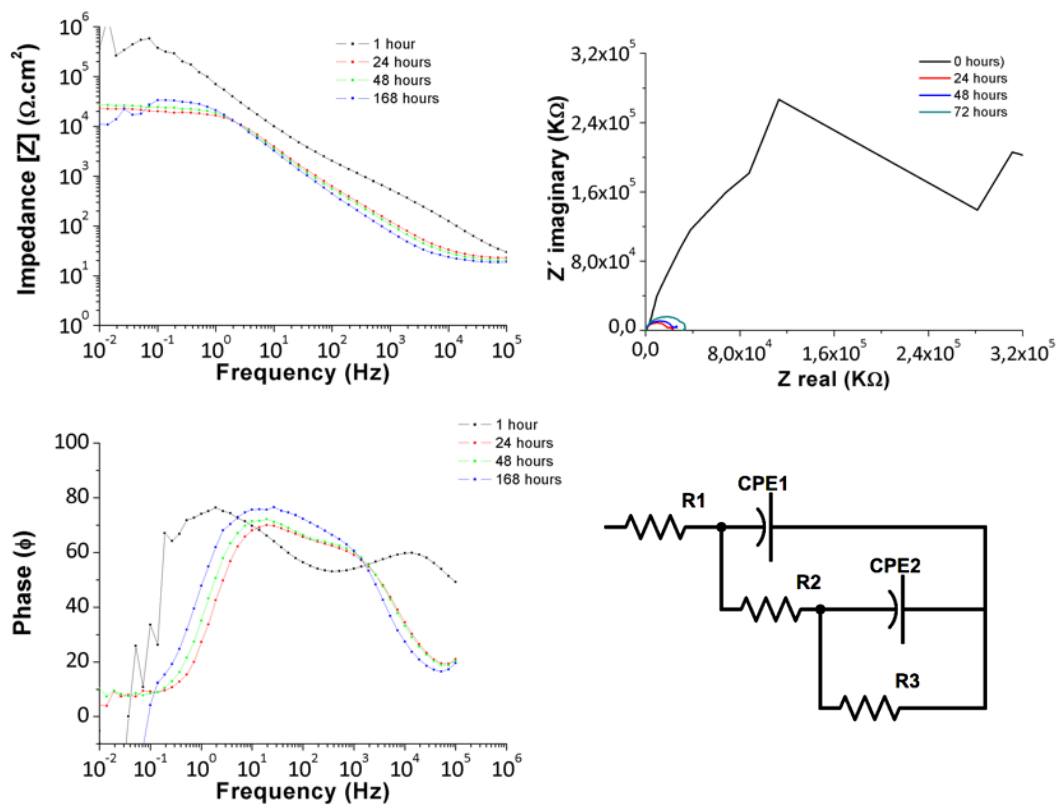
	R1 (Ω·cm ²)	CPE1 (F/cm)	α ₁	R2 (Ω·cm ²)	CPE2 (F/cm)	α ₂	R3 (Ω·cm ²)
1h	47.2	2.36E-07	0.85991	116.1	1.91E-06	0.87725	3.24E+05
24h	19.46	8.18E-07	0.86792	24.54	4.54E-06	0.87213	52724
48h	15.27	6.85E-07	0.85662	20.43	5.68E-06	0.85546	42164
168h	4.753	1.22E-06	0.84799	8.394	1.45E-05	0.8429	21148

Sample 4: GPTMS+MTEOS+Graphene Oxide,1 dip + PFAS, 1 dip



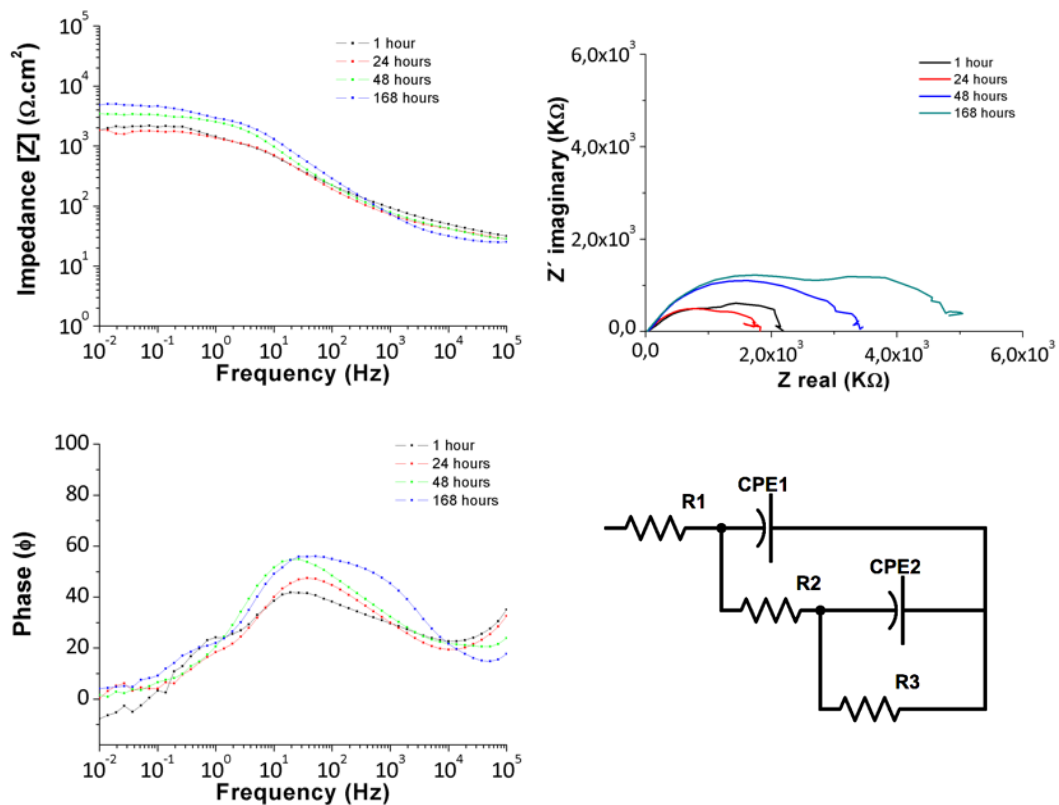
	R1 ($\Omega\cdot\text{cm}^2$)	CPE1 (F/cm)	α_1	R2 ($\Omega\cdot\text{cm}^2$)	CPE2 (F/cm)	α_2	R3 ($\Omega\cdot\text{cm}^2$)
1h	21.33	1.02E-06	0.89741	56.91	2.52E-06	0.89344	1.16E+05
24h	20.86	5.77E-06	0.87082	118.3	4.11E-06	0.89958	23069
48h	18.34	1.08E-05	0.82986	470.5	3.02E-06	0.94793	26270
168h	7.896	3.55E-05	0.8197	247.8	1.28E-05	0.9	3.621

Sample 5: GPTMS+MTEOS+Graphene Oxide, 1 dip + PFAS, 1 dip + HEAT TREATMENT

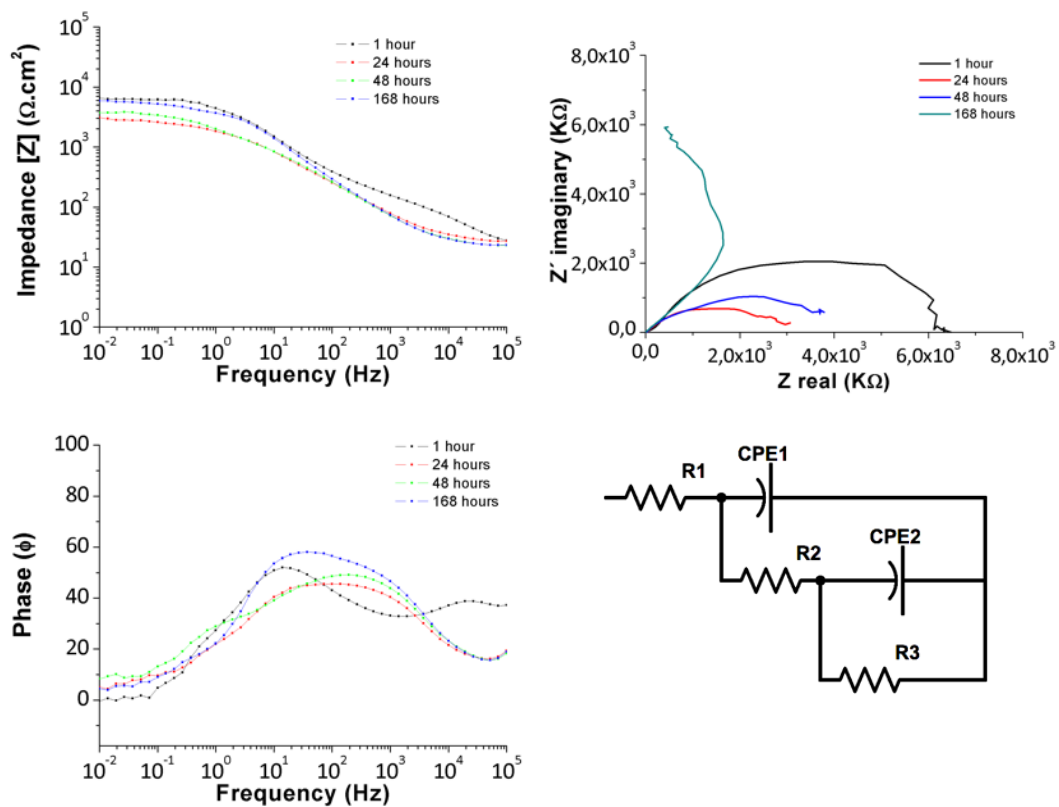


	R1 (Ω·cm ²)	CPE1 (F/cm)	α ₁	R2 (Ω·cm ²)	CPE2 (F/cm)	α ₂	R3 (Ω·cm ²)
1h	6.179	3.22E-06	0.78893	811.7	2.90E-06	0.91504	2.74E+05
24h	21.31	5.20E-06	0.83499	733.3	1.60E-06	0.93	2.8374
48h	19.58	4.83E-06	0.85952	594.8	2.28E-06	0.91	3.0501
168h	7.941	1.15E-05	0.89924	203.6	4.06E-06	0.9606	13942

Sample 6: GPTMS+MTEOS+TiO₂, 1 dip + PFAS, 1 dip

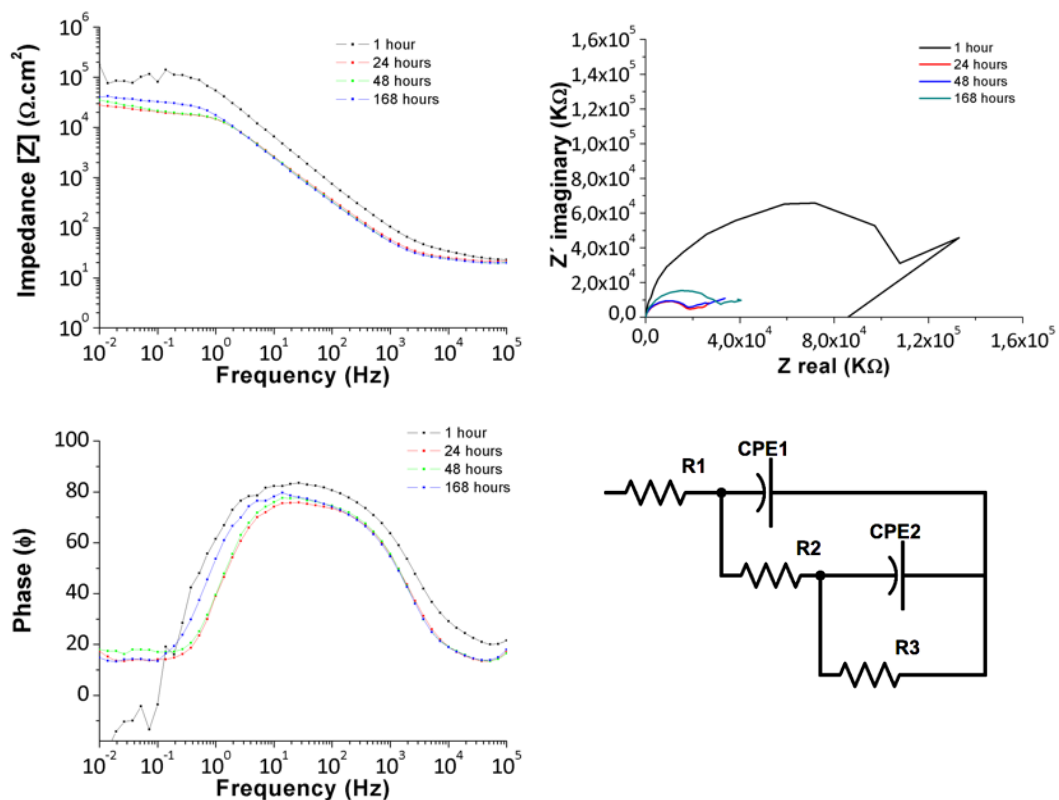


	R1 (Ω·cm ²)	CPE1 (F/cm)	α ₁	R2 (Ω·cm ²)	CPE2 (F/cm)	α ₂	R3 (Ω·cm ²)
1h	2.343	1.50E-05	0.56005	60.56	9.83E-05	0.59104	2304
24h	6.89E-08	1.75E-05	0.54248	52.09	6.15E-05	0.68061	1789
48h	20.58	1.36E-05	0.68306	54.06	3.18E-05	0.74451	3358
168h	9.961	5.78E-05	0.67361	6.50E-08	3.82E-05	0.69196	2069

Sample 7: GPTMS+MTEOS+TiO₂, 1 dip + PFAS, 1 dip + HEAT TREATMENT

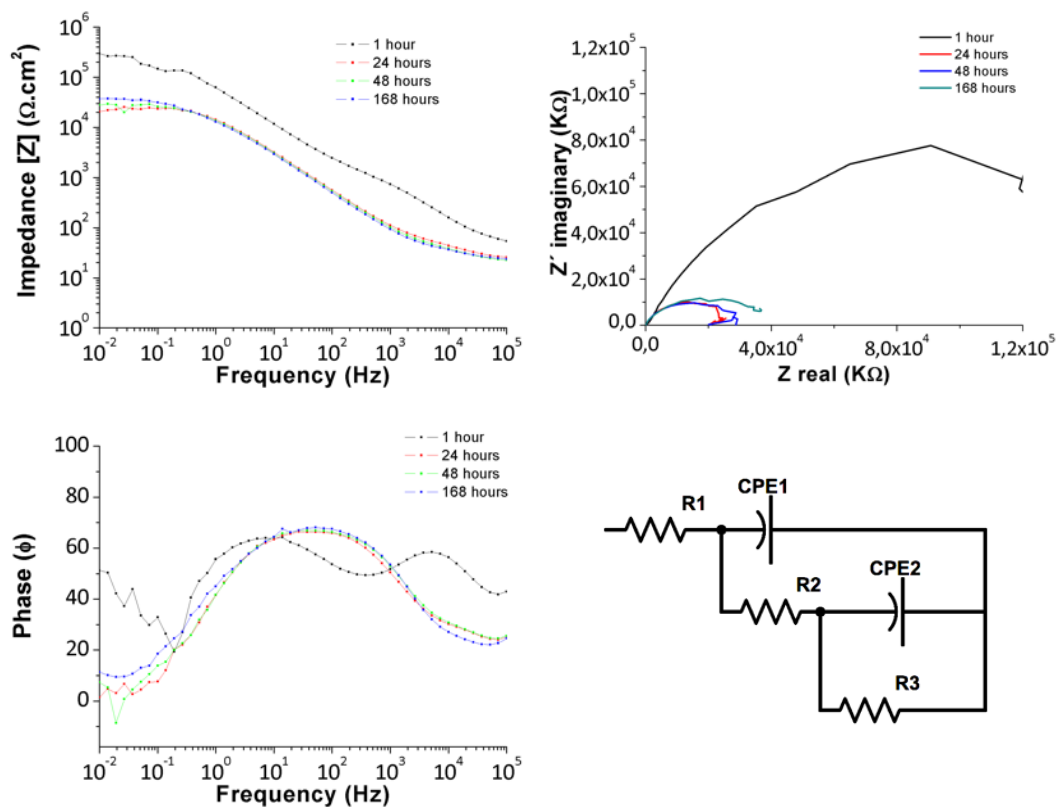
	R1 ($\Omega \cdot \text{cm}^2$)	CPE1 (F/cm)	α_1	R2 ($\Omega \cdot \text{cm}^2$)	CPE2 (F/cm)	α_2	R3 ($\Omega \cdot \text{cm}^2$)
1h	10.7	1.36E-05	0.62426	224.6	1.95E-05	0.75418	6441
24h	4.61E-07	6.17E-05	0.40462	32.85	4.61E-05	0.65256	3102
48h	10.55	0.00012172	0.46839	27.87	8.23E-06	0.80104	4596
168h	3.378	2.59E-06	0.75884	7.575	7.43E-05	0.71039	2410

Sample 8: PFAS, 1 dip



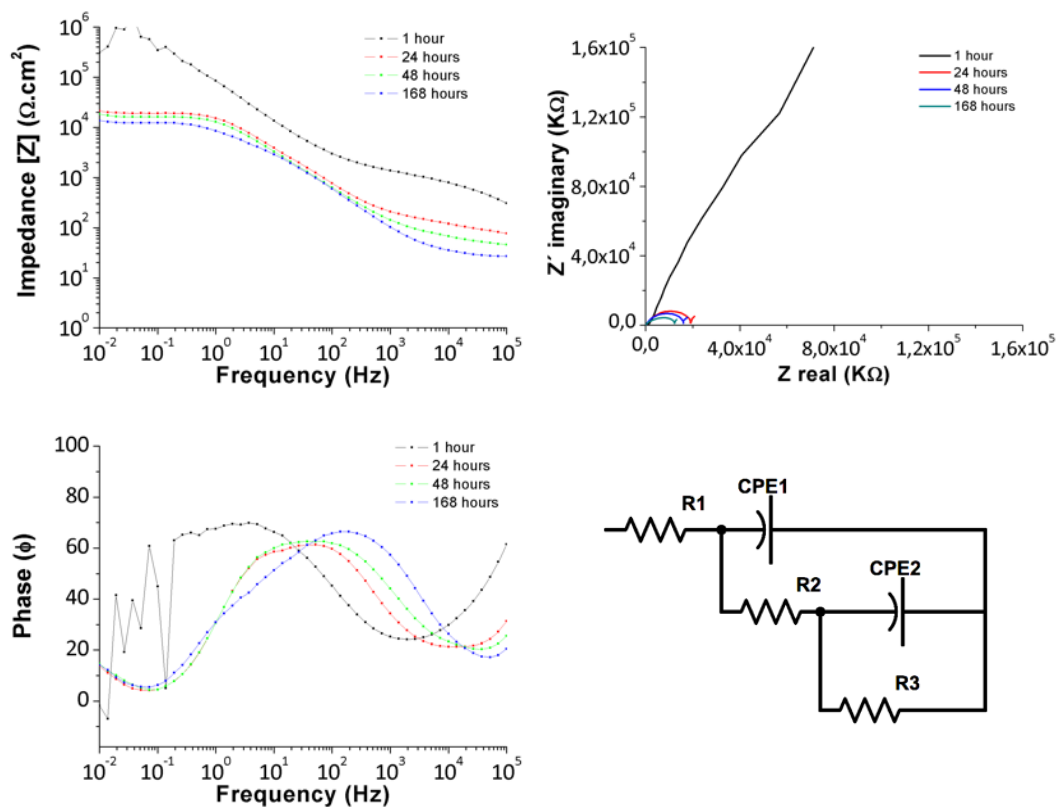
	R1 ($\Omega \cdot \text{cm}^2$)	CPE1 (F/cm)	α_1	R2 ($\Omega \cdot \text{cm}^2$)	CPE2 (F/cm)	α_2	R3 ($\Omega \cdot \text{cm}^2$)
1h	19.42	8.08E-07	0.94812	29.84	2.22E-06	0.93829	1.34E+05
24h	15.62	1.10E-06	0.89966	10.84	8.35E-06	0.87926	21815
48h	15.02	1.09E-06	0.9204	10.12	8.54E-06	0.88607	23502
168h	6.656	3.01E-06	0.90713	4.769	1.90E-05	0.8917	15750

Sample 9: GPTMS+MTEOS, 6 dips



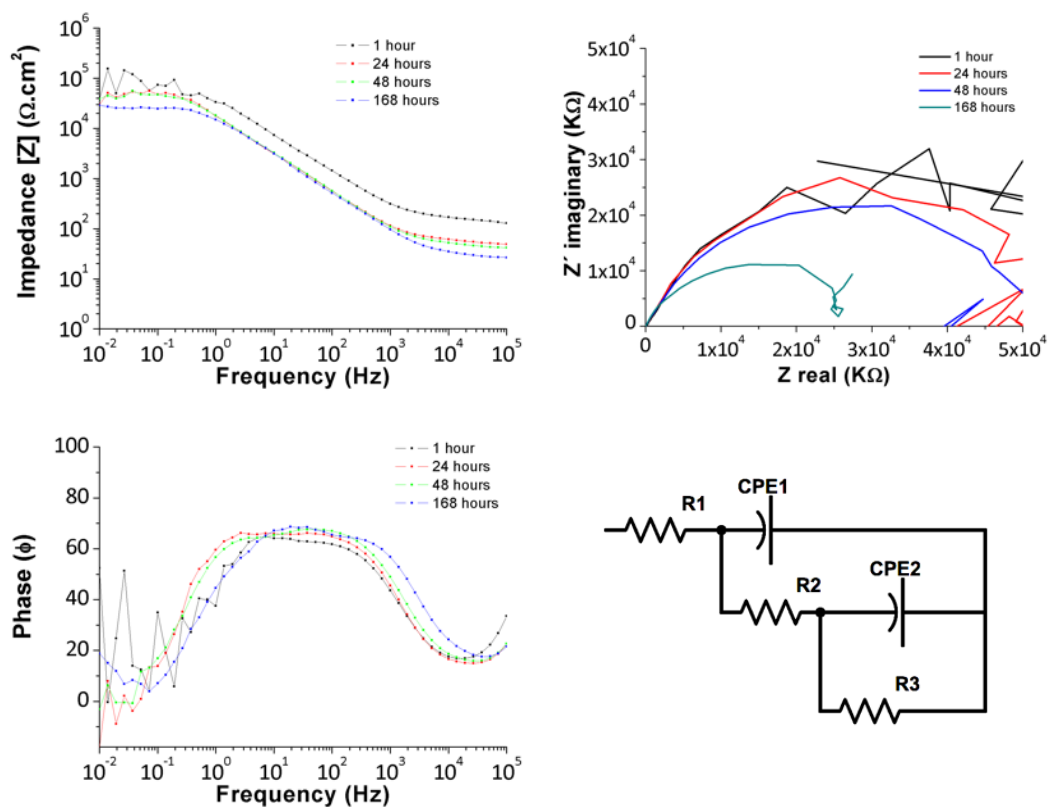
	R1 ($\Omega \cdot \text{cm}^2$)	CPE1 (F/cm)	α_1	R2 ($\Omega \cdot \text{cm}^2$)	CPE2 (F/cm)	α_2	R3 ($\Omega \cdot \text{cm}^2$)
1h	21.9	3.28E-06	0.68571	4755	6.01E-07	0.9361	2.39E+05
24h	17.61	3.06E-06	0.7861	45.62	8.22E-06	0.79065	26148
48h	13.8	6.77E-06	0.72397	43.79	6.09E-06	0.81719	29159
168h	5.305	2.76E-05	0.65634	16.47	9.70E-06	0.87156	17296

Sample 10: GPTMS+MTEOS+Graphene Oxide, 6 dips



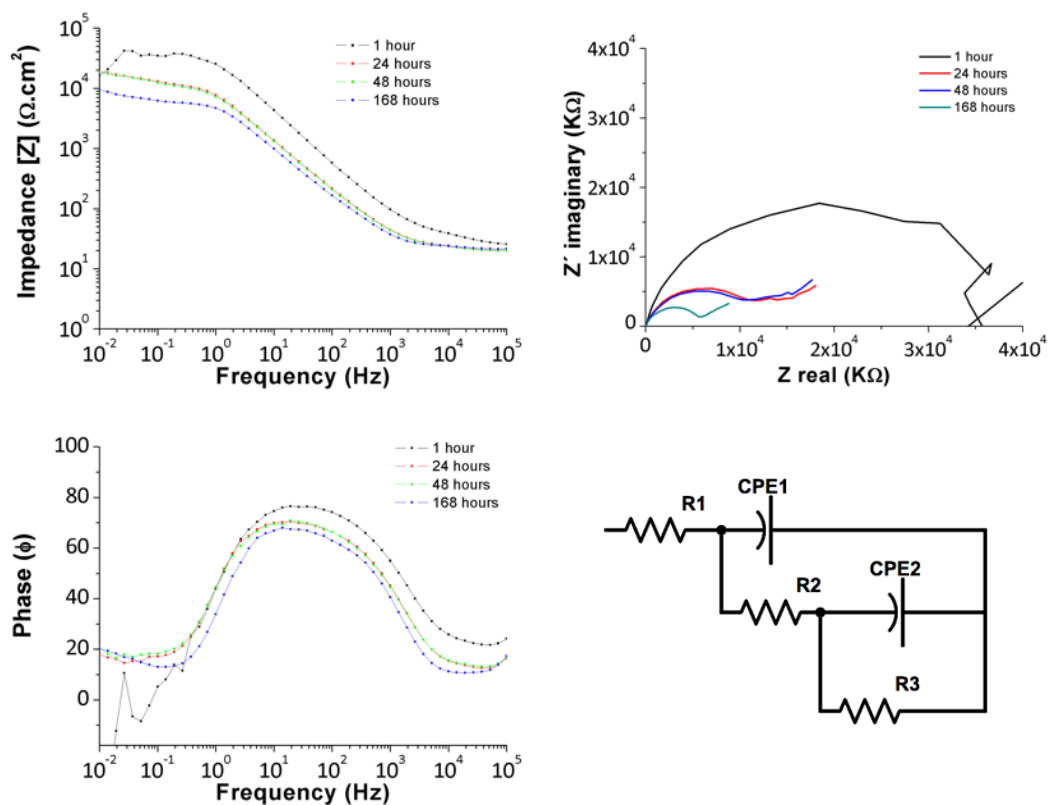
	R_1 ($\Omega \cdot \text{cm}^2$)	CPE_1 (F/cm)	α_1	R_2 ($\Omega \cdot \text{cm}^2$)	CPE_2 (F/cm)	α_2	R_3 ($\Omega \cdot \text{cm}^2$)
1h	26.21	3.70E-07	0.68911	1453	1.84E-06	0.8559	6.96E+05
24h	43.13	1.38E-06	0.73817	112.4	7.50E-06	0.79259	20801
48h	30.8	1.73E-06	0.78304	52.31	8.86E-06	0.78206	17588
168h	11.36	1.96E-05	0.80356	12.57	2.76E-05	0.46405	6202

Sample 11: GPTMS+MTEOS+TiO₂, 6 dips



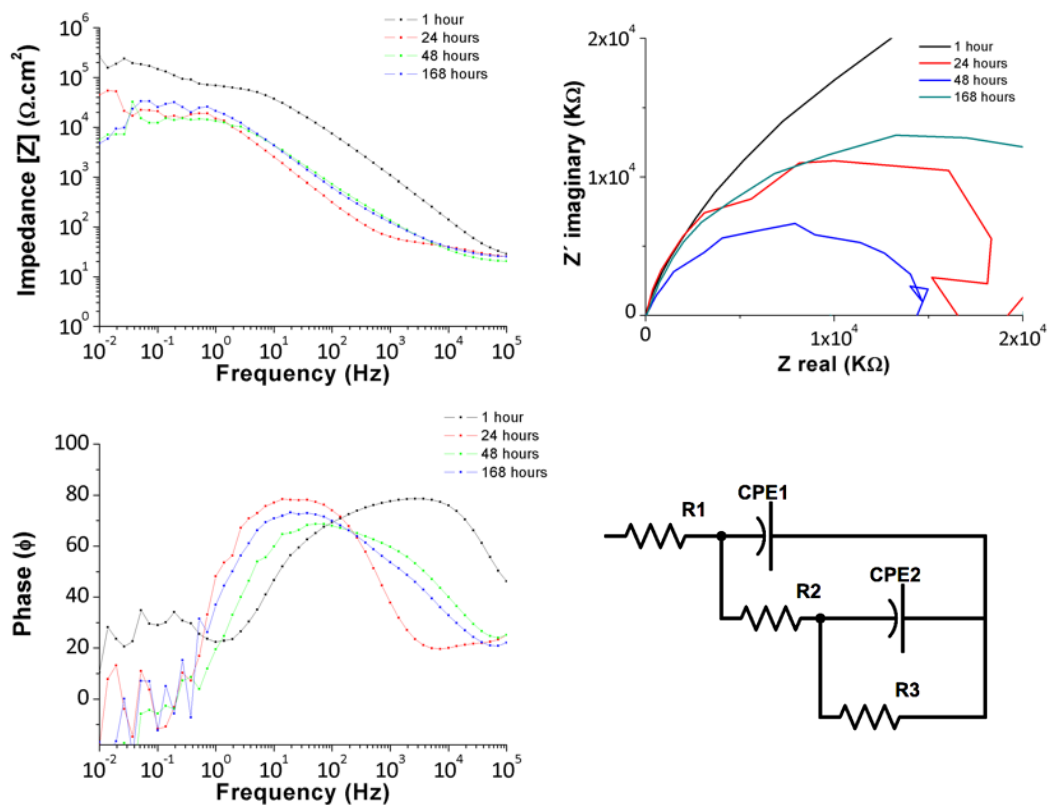
	R1 (Ω·cm ²)	CPE1 (F/cm)	α ₁	R2 (Ω·cm ²)	CPE2 (F/cm)	α ₂	R3 (Ω·cm ²)
1h	31.08	7.30E-09	1.032	118.4	5.68E-06	0.75526	85853
24h	21.06	4.72E-07	0.81152	39.17	1.02E-05	0.80515	60931
48h	3.321	3.64E-07	0.77491	45.35	1.06E-05	0.79677	55382
168h	2.574	9.84E-07	0.81201	10.76	2.44E-05	0.79862	12807

Sample 12: GPTMS+MTEOS+Graphene Oxide, 6 dips + PFAS, 6 dips



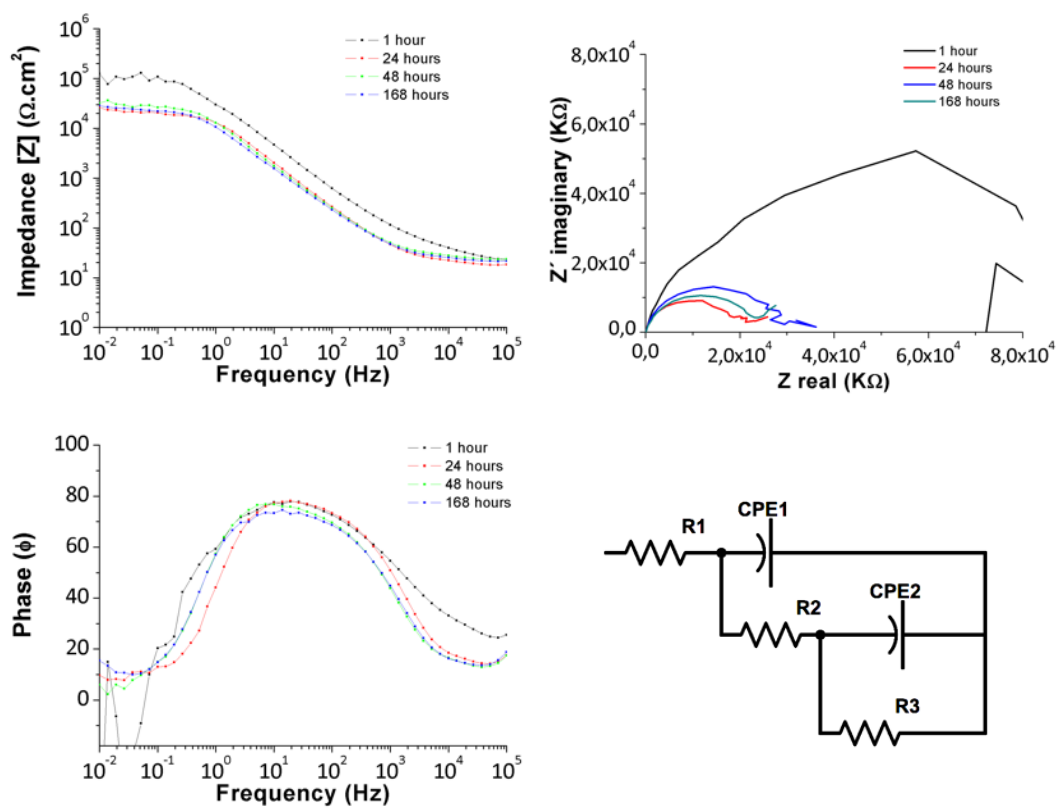
	R1 ($\Omega\cdot\text{cm}^2$)	CPE1 (F/cm)	α_1	R2 ($\Omega\cdot\text{cm}^2$)	CPE2 (F/cm)	α_2	R3 ($\Omega\cdot\text{cm}^2$)
1h	19.84	1.07E-06	0.8923	30.98	4.54E-06	0.88769	38154
24h	21.06	4.72E-07	0.81152	39.17	1.02E-05	0.80515	60931
48h	11.16	5.34E-06	0.72791	13.57	1.99E-05	0.83469	14276
168h	2.259	7.24E-07	0.84539	7.764	7.03E-05	0.82208	3015

Sample 13: GPTMS+MTEOS+Graphene Oxide, 6 dips + PFAS, 6 dips + HEAT TREATMENT



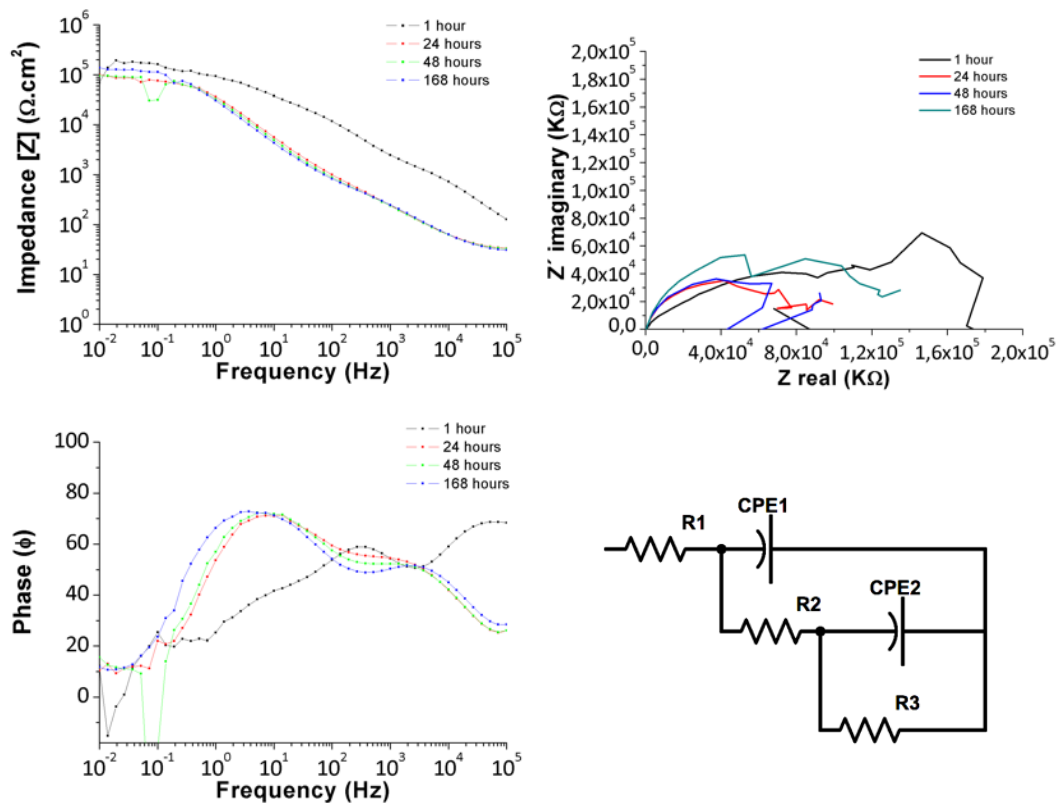
	R1 ($\Omega \cdot \text{cm}^2$)	CPE1 (F/cm)	α_1	R2 ($\Omega \cdot \text{cm}^2$)	CPE2 (F/cm)	α_2	R3 ($\Omega \cdot \text{cm}^2$)
1h	13.9	4.58E-07	0.87461	57929	1.18E-05	0.5857	9.29E+05
24h	19.2	1.12E-06	0.88384	31.21	6.92E-06	0.9421	20427
48h	17.31	3.74E-06	0.83243	172.7	2.53E-06	0.84213	15454
168h	10.23	7.05E-06	0.85657	64.81	6.37E-06	0.89151	12938

Sample 14: GPTMS+MTEOS+TiO₂, 6 dips + PFAS, 6 dips + PFAS, 6 dips



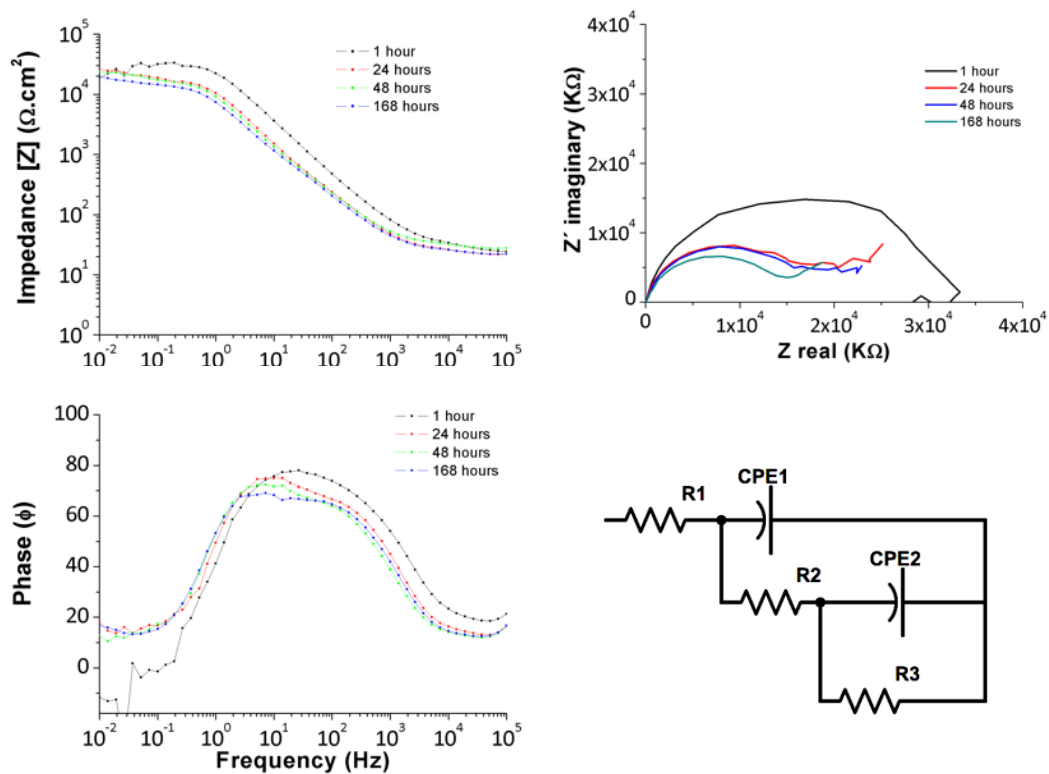
	R1 ($\Omega\cdot\text{cm}^2$)	CPE1 (F/cm)	α_1	R2 ($\Omega\cdot\text{cm}^2$)	CPE2 (F/cm)	α_2	R3 ($\Omega\cdot\text{cm}^2$)
1h	19.14	1.82E-06	0.87042	62.03	3.86E-06	0.87566	1.20E+05
24h	14.87	1.99E-06	0.90936	12.11	9.42E-06	0.89521	20920
48h	20.06	2.53E-06	0.89107	15.87	1.12E-05	0.88167	30723
168h	7.27	5.28E-06	0.86718	5.558	3.42E-05	0.85731	11257

Sample 15: GPTMS+MTEOS+TiO₂ ,6 dips + PFAS, 6 dips + PFAS, 6 dips + HEAT TREATMENT



	R1 ($\Omega \cdot \text{cm}^2$)	CPE1 (F/cm)	α_1	R2 ($\Omega \cdot \text{cm}^2$)	CPE2 (F/cm)	α_2	R3 ($\Omega \cdot \text{cm}^2$)
1h	35	1.03E-06	0.80271	1347	1.11E-06	0.95863	80256
24h	29	3.90E-06	0.78289	1172	1.41E-06	0.94889	82065
48h	27.95	3.93E-06	0.78251	929	1.88E-06	0.94817	86492
168h	10.85	8.70E-06	0.77612	367	6.23E-06	0.92934	61014

Sample 16: PFAS, 6 dips



	R1 ($\Omega \cdot \text{cm}^2$)	CPE1 (F/cm)	α_1	R2 ($\Omega \cdot \text{cm}^2$)	CPE2 (F/cm)	α_2	R3 ($\Omega \cdot \text{cm}^2$)
1h	20.24	1.25E-06	0.90752	25.29	4.96E-06	0.89762	33585
24h	17.69	2.58E-06	0.87046	12.95	1.48E-05	0.85373	21125
48h	21.85	2.53E-06	0.84842	14.81	1.85E-05	0.8369	20517
168h	6.659	4.78E-06	0.82867	5.19	5.50E-05	0.81762	7476

5.1.4. Glow Discharge Emission Spectrometry results

In order to characterise the distribution of the layers and the components of the coating, a glow discharge emission spectrometry (GDOES) tests was performed. GDOES is used to determine the concentration of the elements of a sample. It s a powerful tool to obtain the distribution of the elements on the surface of a solid.

In the following charts the composition of two coatings is shown. The first of them is the GPTMS+MTEOS+GrOx+PFAS 6 dips sample. It can be seen how the initial layer contains carbon, oxygen and silica from the sol-gel matrix, carbon from the graphene oxide and fluorine from the PFAS coating. The concentration of these elements decrease as depth is increased, where aluminum is the predominant element.

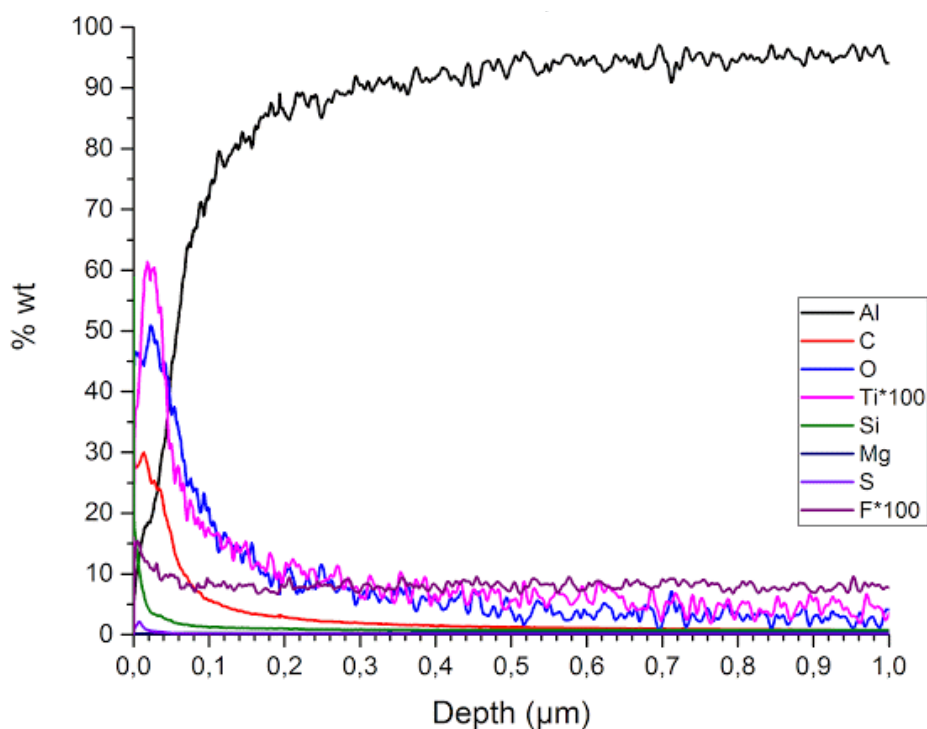


Fig 39. GPTMS+MTEOS+GrOx+PFAS GDOES analysis

Note that the titanium and fluorine concentrations have been multiplied by a 100 factor to be visible on the graph.

Another GDOES analysis was performed on the GPTMS+MTEOS+TiO₂+PFAS 6 dips sample. In this graph the limit between the sol-gel coating and the substrate is clearly differentiated. The concentrations of titanium, carbon, oxygen and silica is greater in the coating part. See how in the very outer part of the layer the concentration of carbon is smaller and the concentration of fluorine increases. This clearly illustrates how the fluorinated chains are disposed to the exterior to form the hydrophobic layer. Titanium concentration starts to increase once the PFAS layer is passed.

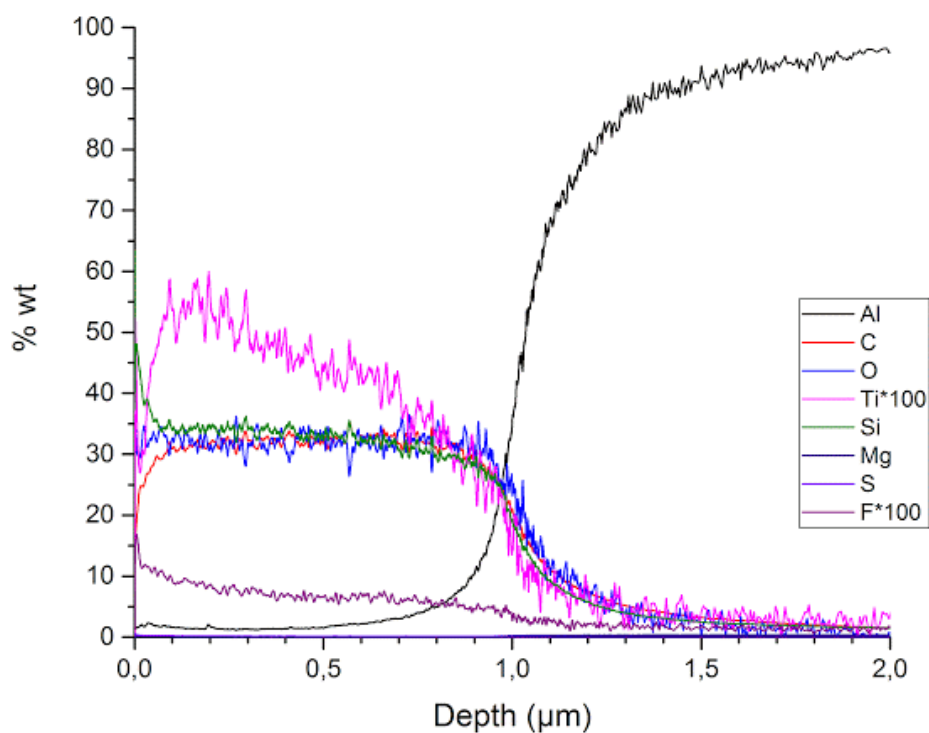


Fig 40. GPTMS+MTEOS+TiO₂+PFAS GDOES analysis

5.2. Analysis and discussion of results

5.2.1. Number of dips

The number of dips of the sol-gel coating directly influences its corrosion resistance. As it can be seen on the following graphs, those samples with 6 dips have considerably better corrosion resistance than those with a single dip. This can be seen on the coating resistance (R_2 in the equivalent circuit). Let us recall that the coating resistance models the electronic/ionic conductivity and represent a charge transference.

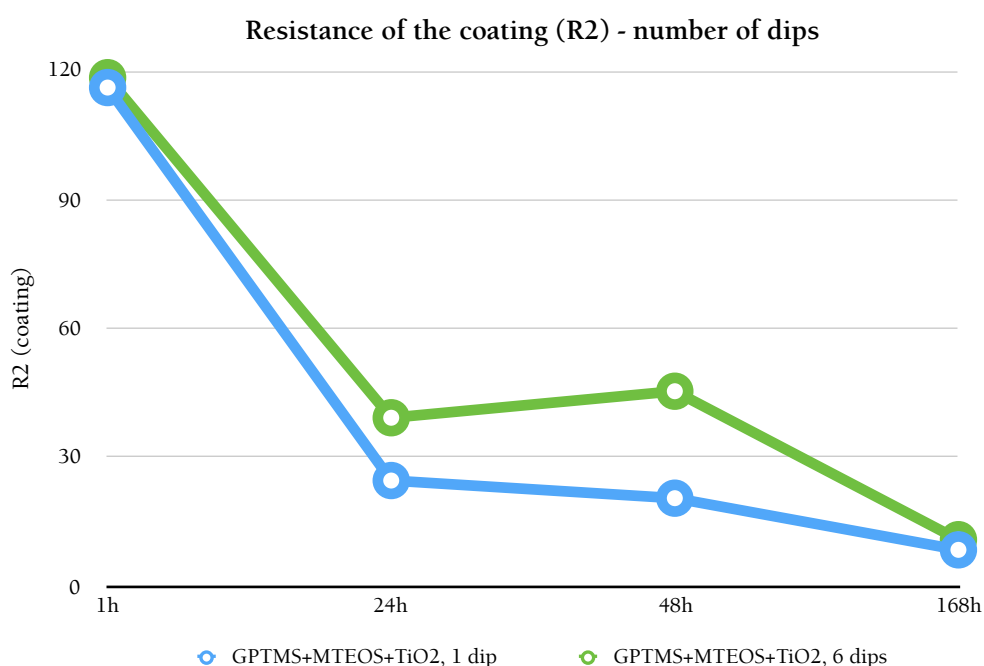


Fig 41. 1 dip - 6 dips R_2 comparison

The previous graph shows how, when the samples are just submerged on the NaCl solution, the initial resistance is almost the same, since the electrolyte has not yet diffused. As time passes, the 6 dips coating shows a better behaviour; at 48 hours the resistance even increases due to the double layer formed by corrosion products. At the one week interval, electrolyte has diffused and both resistances are equaled.

The coating capacitance also illustrates the behaviour of the coating with time. It represents the diffusion of the electrolyte into the coating, and the greater the capacitance, the more the electrolyte has diffused. The following graph shows the evolution of the capacitance of the 1 and 6 dip samples. Note that in both of the samples the capacitance increases with time, but at 48 hours the corrosion products reduce momentarily the

capacitance. As it can be seen, the capacitance of the 6 dips coating is considerably lower than the one of the 1 dip coating.

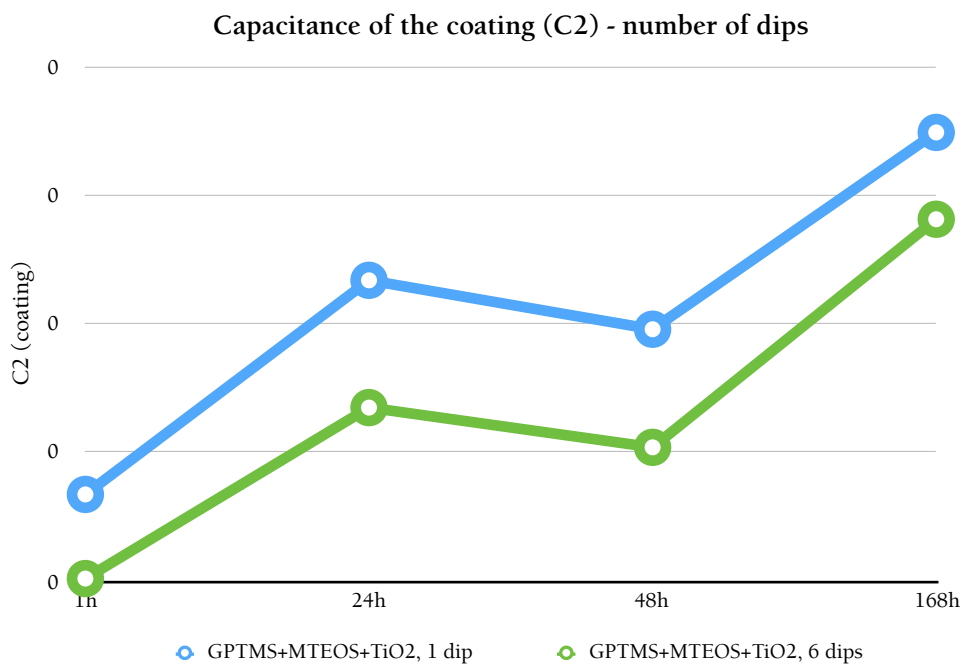


Fig 42. 1 dip - 6 dips C2 comparison

The results show that, as it can be intuitively expected, that the coating with a greater number of layers has a better corrosion resistance than the one with just one layer.

5.2.2. Heat treatment

A heat treatment of 180°C overnight was applied to some of the samples in order to obtain a more stable coating. The thermal treatment helps to form the hydrogen bonds and the resulting coating is more compact. The effect of the heat treatment on the corrosion resistance is illustrated through the following graph. The coating resistance (R2) is significantly higher than the one of the same coating but without heat treatment.

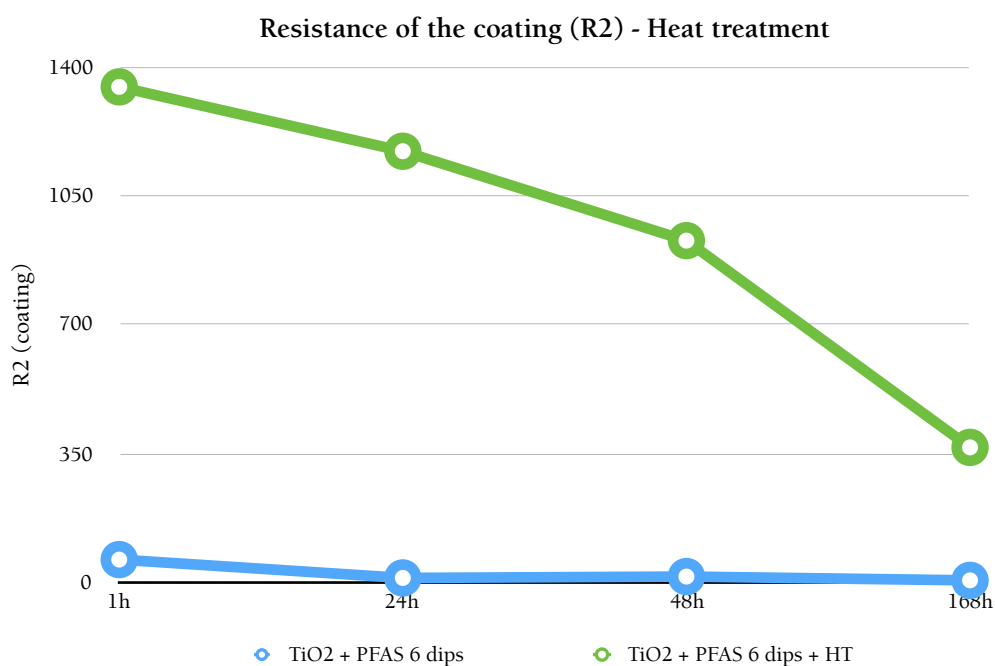


Fig 43. Heat treatment R2 comparison

5.2.3. Inhibitor

The results prove that both inhibitors enhance corrosion resistance compared to the bare aluminium substrate. The corrosion resistance is also greater than that of the GPTMS +MTEOS coating, without inhibitor. However, as it can be seen in the following graphs, the TiO₂ coatings present a slightly better anticorrosion behaviour.

The following graph shows the overall comparison between TiO₂ and graphene oxide, according to the pitting corrosion tests results:

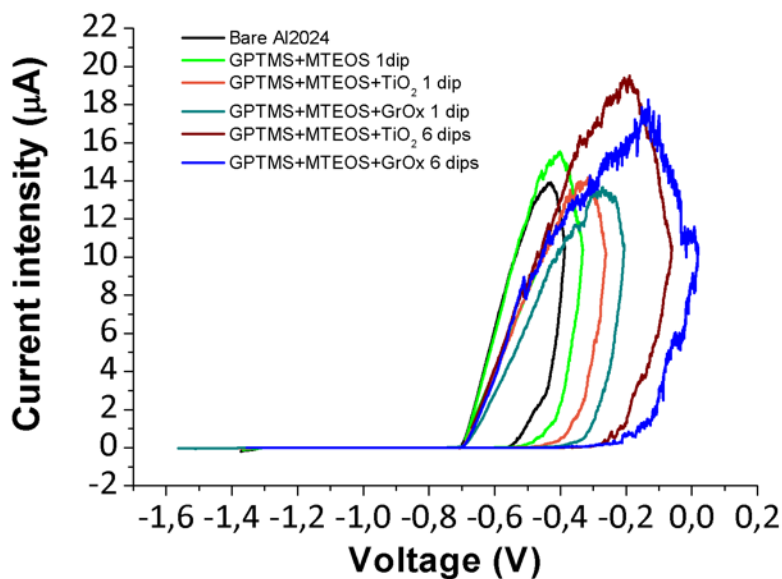


Fig 44. Graphene oxide overall comparison

This can be also seen in the evolution of the equivalent circuit parameters. TiO₂ coating resistance (R2) has a better behaviour than the graphene oxide.

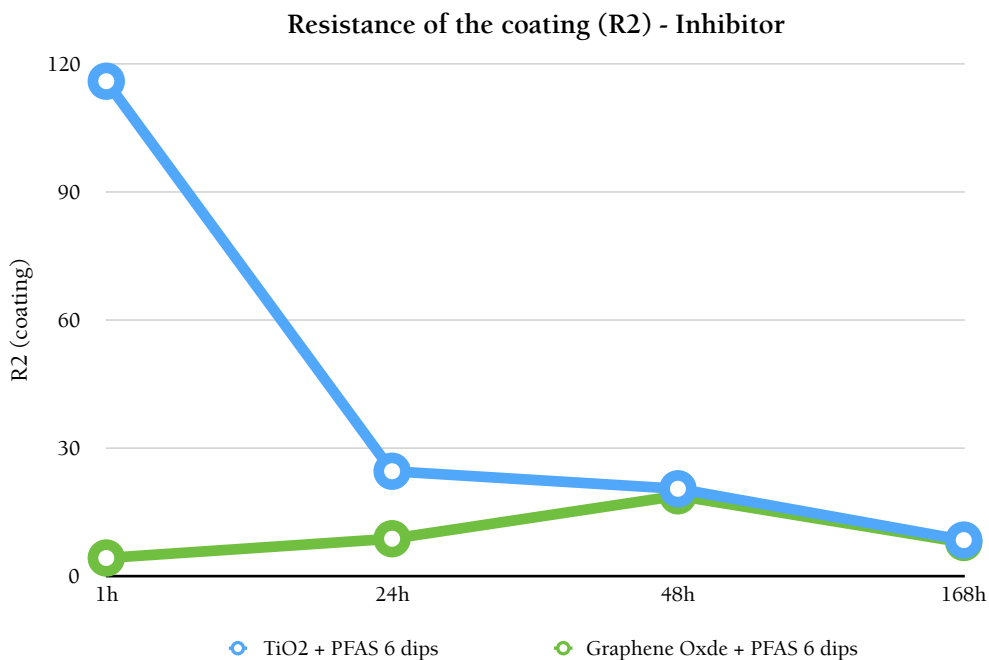


Fig 45. Inhibitor - R2 comparison

5.2.4. Hydrophobicity

The results obtained from the pitting corrosion and electrochemical impedance spectroscopy tests prove that there is a relationship between the hydrophobicity and the corrosion resistance of the coatings. The values obtained from those tests are compared with the water contact angles of the samples, in order to illustrate this relationship.

As it is shown in the following pages, a higher water contact angle generally leads to a better corrosion resistance. The first graph shows the overall behaviour of the samples with graphene oxide. A table is attached to illustrate the relationship between the pitting potential and the water contact angle of each of the samples.

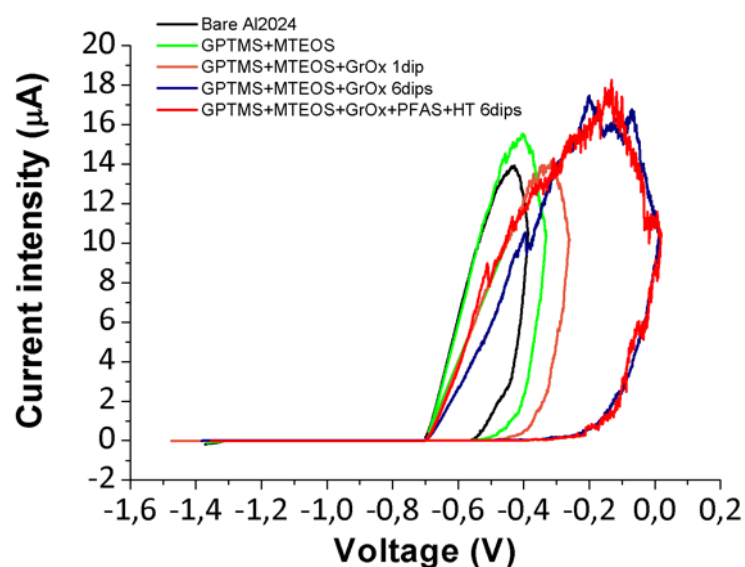


Fig 46. Pitting potential of the Graphene oxide samples

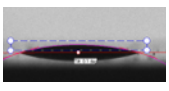
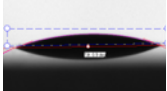
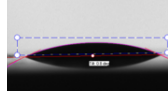
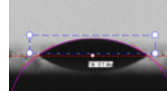
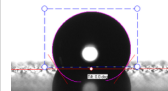
Sample	Control, no coating	GPTMS +MTEOS 1 dip	GPTMS +MTEOS +GrOx 1 dip	GPTMS +MTEOS +GrOx 6 dip	GPTMS +MTEOS +GrOx +PFAS 6 dip +HT.
Pitting voltage (V)	-0.57	-0.54	-0.52	-0.33	-0.29
WCA (°)	17.14	22.16	24.37	35.89	124.87
					

Table 8. Pitting potential - WCA relationship for Graphene oxide samples

This can be also seen through the evolution of the parameters of the equivalent circuit. As an example, the coating resistance of the TiO₂ + PFAS coating presents higher values than the one without PFAS. The water contact angle of each of the samples is TiO₂ WCA = 94.52° and TiO₂ + PFAS + HT WCA = 120.04°.

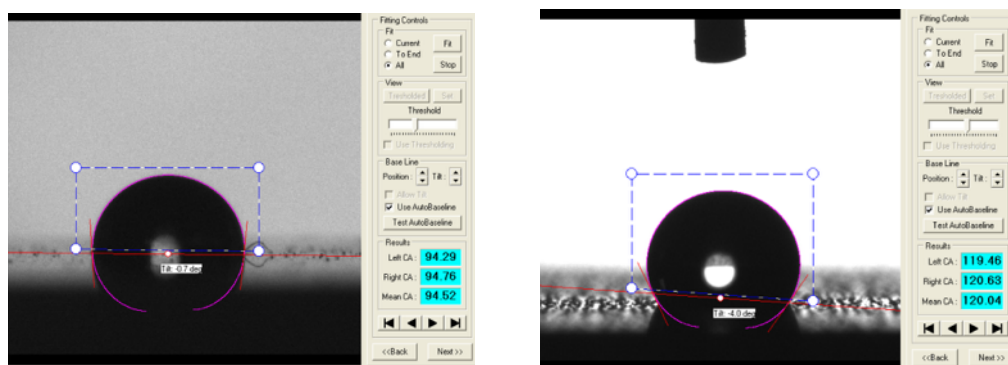


Fig 47. TiO₂ WCA = 94.52° and TiO₂ + PFAS + HT WCA = 120.04°.

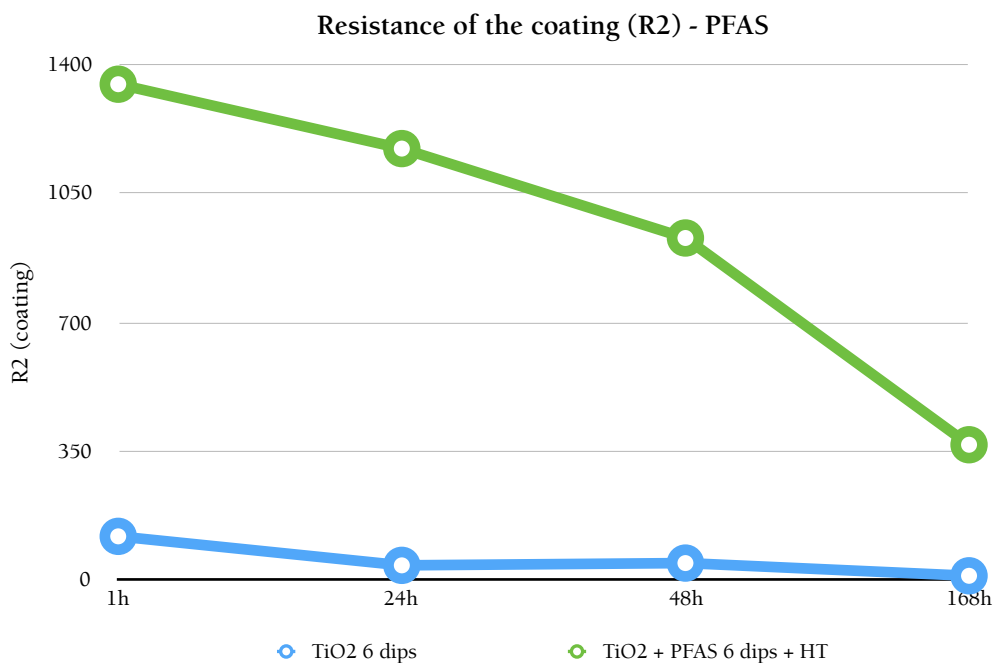


Fig 48. Inhibitor - R2 comparison

The following chart shows the evolution of the coating capacitance C2 of the graphene oxide samples, one of them with an additional PFAS coating. Note that the capacitance of the sample without PFAS increases with time more drastically than the one with PFAS. The water contact angle of each of the samples is: Graphene Oxide WCA = 36.24° and Graphene Oxide + PFAS + HT WCA = 124.87°.

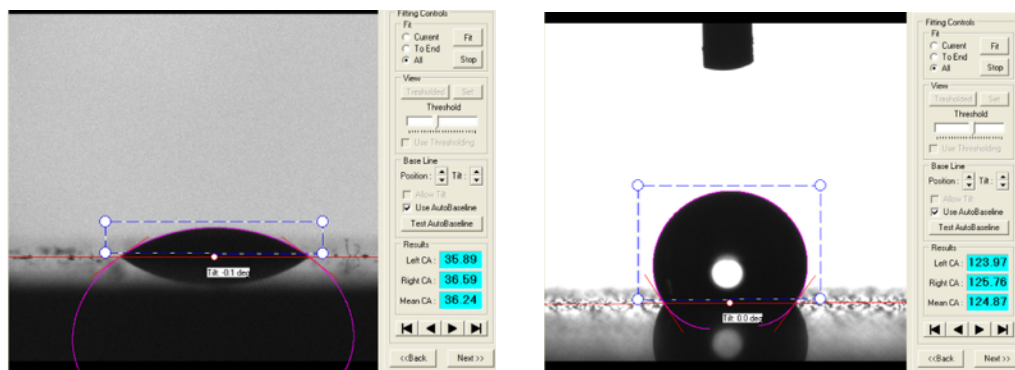


Fig 49. Graphene Oxide WCA = 36.24° and Graphene Oxide + PFAS + HT WCA = 124.87°.

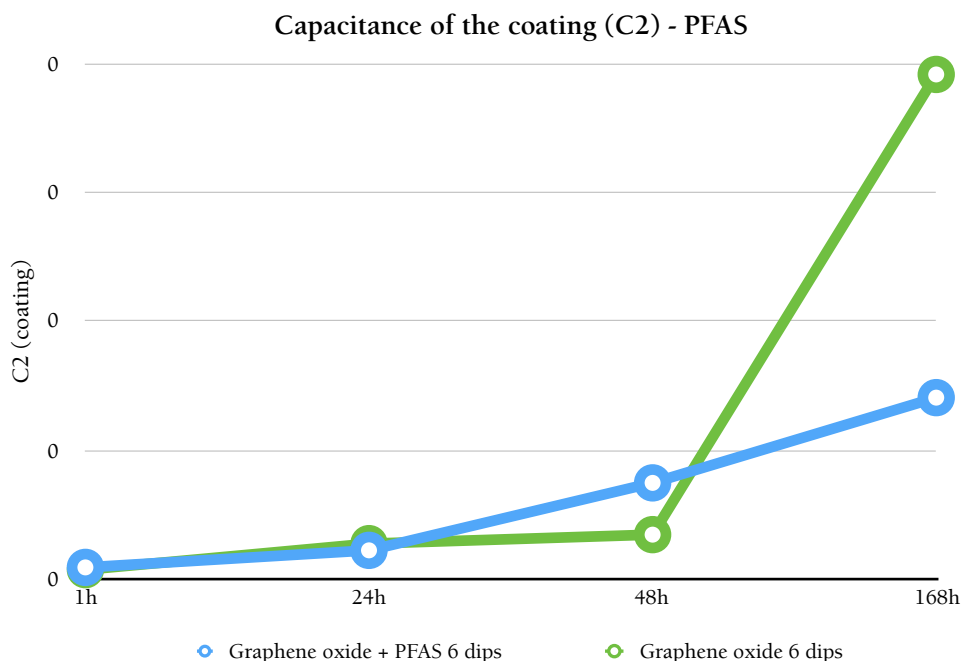


Fig 50. PFAS-C2 comparison

5.2.5. Solubility of the electrospinning fibers

Electrospinning is a very promising technique to obtain anti-corrosion coatings. The fibrous coating provides a rough base layer, ideal to increase the hydrophobicity of the coating. In this project electrospinning fibers were successfully spun and the corrosion inhibitor was accepted by the matrix without precipitation.

After the cross-linking process, both chemical (with acetone) and thermal, an stable and rubbing-free coating was obtained. Nevertheless, the fibers were soluble in water and further coatings were not able to be deposited. The PVA-PVPON-SDS recipe produces polar fibers that are easily solved in water.

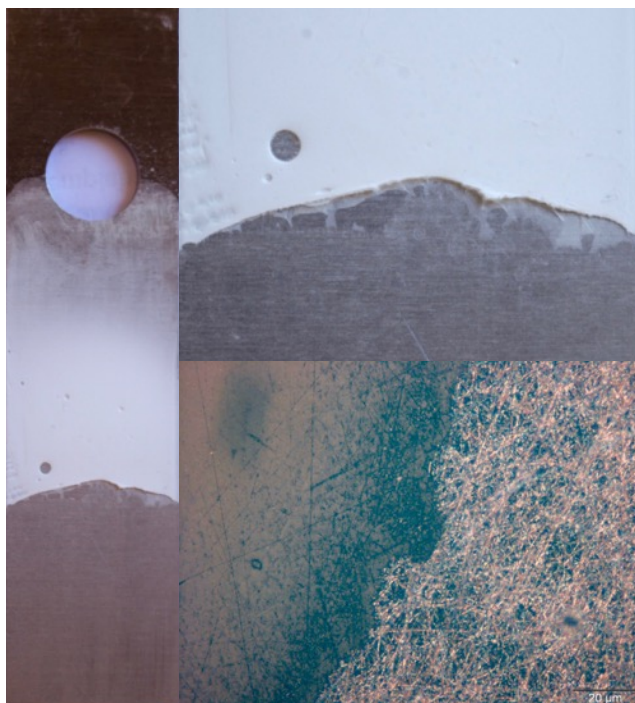


Fig 51. Sample with electrospinning fibers after being partially submerged in water. General and microscope view.

6. Conclusions and open research lines

- The chemical kinetics of sol-gel reactions that take place on a basic medium are significantly faster than those that take place in an acid medium. Therefore the control of the viscosity of the gel in order to make depositions is simpler in an acid medium.
- More than a single dip is needed to obtain an effective coating, since with only one dip the structure of the surface is not enough consistent and hierarchical.
- An excess on the inhibitor in the sol-gel matrix can promote the formation of cracks and holes in the coating and therefore the sol-gel structure losses its coherency.
- The industrial application of sol-gel coatings for corrosion protection is still developing. Its large-scale viability and applications must be deeply studied but some advantages are obvious, like the possibility of obtaining homogenous coating depositions on complex geometries.
- More stable and compact coatings are obtained after a heat treatment.
- Hydrophobicity is an important factor in order to develop anticorrosion coatings.
- In multilayer coatings the presence of a corrosion inhibitor behind an hydrophobic layer enhances its anticorrosion behaviour.
- An optimization of the hydrophobic sol-coatings will lead to greater contact angles and, as it has been shown, to a better corrosion resistance of the coating.
- A fibrous electrospinning base coating can increase the roughness of the coating and therefore its hydrophobicity.
- It is necessary an optimization of the cross linking process of the electrospinning fibers and the development of apolar fibers.

Bibliography

1. Fontana, M.G., *Corrosion Engineering*. 3 ed. 1987, New York: McGraw-Hill.
2. Larsson, A., *STEELCOAT Report Summary*, European Commission, Editor. 2014, European Union.
3. Fürbeth, W. and M. Schütze, Progress in corrosion protection as a requirement for technical progress. *Materials and Corrosion*, 2009. **60**(7): p. 481-494.
4. Chang, R., *Chemistry*. 10 ed. 2010, New York: McGraw-Hill.
5. Callister, W.D. and D.G. Rethwisch, *Materials Science And Engineering: An Introduction*. 8 ed. 2010, New Jersey: John Wiley & Sons.
6. Gellings, P.J., *Introduction to corrosion prevention and control*. 1985, Delft: Delft University Press.
7. Gómez de León Hijes, F.C. and D.J. Alcaraz Lorente, *Manual básico de corrosión para ingenieros*. 1 ed. 2004, Murcia: Universidad de Murcia.
8. Otero Huerta, E., *Corrosión y degradación de materiales*. Biblioteca de químicas, ed. Síntesis. 2012, Madrid.
9. Certificación, A.E.d.N.y., CEN, and O.I.d. Normalización, UNE-EN ISO 8044: corrosión de metales y aleaciones : términos principales y definiciones : (ISO 8044:1999). 2000: AENOR.
10. Finšgar, M. and J. Jackson, Application of corrosion inhibitors for steels in acidic media for the oil and gas industry: A review. *Corrosion Science*, 2014. **86**: p. 17-41.
11. Wang, D. and G.P. Bierwagen, Sol-gel coatings on metals for corrosion protection. *Progress in Organic Coatings*, 2009. **64**(4): p. 327-338.
12. UC Rusal. *All about aluminium: economics*. 2016 [cited 2016; Available from: aluminiumleader.com].
13. Totten, G.E., K. Funatani, and L. Xie, *Handbook of metallurgical process design*. 2004: CRC press.
14. ALCOA Mill Products, *ALLOY 2024 Sheet and plate*, ALCOA, Editor. 2015: Bettendorf, Iowa.
15. MatWeb. *Alclad Aluminum 2024-O*. 2016 [cited 2016; Available from: matweb.com].
16. *Proceso de Anodizado*. 2016; Available from: sapagroup.com.
17. Rosero-Navarro, N.C., *Recubrimientos producidos por sol-gel con inhibidores de corrosión para la protección activa de aleaciones ligeras*. 2011, Universidad Autónoma de Madrid.
18. European Chemicals Bureau, European Union Risk Assessment Report CAS-No.: 1333-82-0, 7775-11-3, 10588-01-9, 7789-09-5 and 7778-50-9 EINECS-No.: 215-607-8, 231-889-5, 234-190-3, 232-143-1 and 231-906-6. 2005, European Communities: Luxembourg.
19. European Chemicals Agency, Services to support the assessment of remaining cancer risks related to the use of chromium- and arsenic-containing substances in Applications for Authorisation, Final report for Hexavalent Chromium. 2013, Consortium ETeSS: Helsinki.
20. Makhlof, A.S.H., *Handbook of smart coatings for materials protection*. 2014: Elsevier.

21. Roberge, P., Corrosion Engineering: Principles and Practice. 2008: McGraw-Hill Education.
22. Dimitriev, Y., Y. Ivanova, and R. Iordanova, *History of sol-gel science and technology*. Journal of the University of Chemical technology and Metallurgy, 2008. 43(2): p. 181-192.
23. Wright, J.D. and N.A. Sommerdijk, Sol-gel materials: chemistry and applications. Vol. 4. 2000: CRC press.
24. Rivero Fuente, P.J., Contribution to the development of functional nanostructured coatings based on silver nanoparticles, in Departamento de Ingeniería Eléctrica y Electrónica. 2014: Pamplona.
25. Celzard, A. and J. Marêché, Applications of the sol-gel process using well-tested recipes. Journal of chemical education, 2002. 79(7): p. 854.
26. Musgo, J., et al., Ammonia-catalyzed silica xerogels: Simultaneous effects of pH, synthesis temperature, and ethanol:TEOS and water:TEOS molar ratios on textural and structural properties. Microporous and Mesoporous Materials, 2009. 118(1-3): p. 280-287.
27. Rivero Fuente, P.J., Estudio de la mojabilidad de recubrimientos transparentes. 2010, Universidad Pública de Navarra.
28. Nadetech Innovation S.L. *Tecnologías, Dip Coating*. Available from: nadetech.com.
29. Collinson, M.M., et al., The effects of drying time and relative humidity on the stability of sol-gel derived silicate films in solution. Journal of Electroanalytical Chemistry, 2002. 519(1-2): p. 65-71.
30. Montemor, M.F., Functional and smart coatings for corrosion protection: A review of recent advances. Surface and Coatings Technology, 2014. 258: p. 17-37.
31. Mohamed, A.M.A., A.M. Abdullah, and N.A. Younan, Corrosion behavior of superhydrophobic surfaces: A review. Arabian Journal of Chemistry, 2015. 8(6): p. 749-765.
32. Wenzel, R.N., Resistance of solid surfaces to wetting by water. Industrial & Engineering Chemistry, 1936. 28(8): p. 988-994.
33. Wenzel, R.N., *Surface Roughness and Contact Angle*. The Journal of Physical Chemistry, 1949. 53(9): p. 1466-1467.
34. Ishizaki, T., Y. Masuda, and M. Sakamoto, Corrosion resistance and durability of superhydrophobic surface formed on magnesium alloy coated with nanostructured cerium oxide film and fluoroalkylsilane molecules in corrosive NaCl aqueous solution. Langmuir, 2011. 27(8): p. 4780-4788.
35. Brassard, J.-D., D. Sarkar, and J. Perron, Synthesis of monodisperse fluorinated silica nanoparticles and their superhydrophobic thin films. ACS applied materials & interfaces, 2011. 3(9): p. 3583-3588.
36. *Sigma-Aldrich*. 2016 [cited 2016; Available from: www.sigmaaldrich.com.
37. Jeong, C., Nano-engineering of superhydrophobic aluminum surfaces for anti-corrosion. 2013.
38. Wankhede, R.G., et al., Development of water-repellent organic-inorganic hybrid sol-gel coatings on aluminum using short chain perfluoro polymer emulsion. Applied Surface Science, 2013. 283: p. 1051-1059.
39. Lee, J.-W. and W. Hwang, Exploiting the silicon content of aluminum alloys to create a superhydrophobic surface using the sol-gel process. Materials Letters, 2016. 168: p. 83-85.

40. Sánchez, L.M.D., L. Rodríguez, and M. López, *Electrospinning: la era de las nanofibras*. Revista Iberoamericana de Polímeros, 2013. 14(1): p. 10-27.
41. Bhardwaj, N. and S.C. Kundu, Electrospinning: A fascinating fiber fabrication technique. Biotechnology Advances, 2010. 28(3): p. 325-347.
42. Frenot, A. and I.S. Chronakis, *Polymer nanofibers assembled by electrospinning*. Current Opinion in Colloid & Interface Science, 2003. 8(1): p. 64-75.
43. Leach, M.K., et al., Electrospinning Fundamentals: Optimizing Solution and Apparatus Parameters. Journal of Visualized Experiments : JoVE, 2011(47): p. 2494.
44. Huang, Z.-M., et al., A review on polymer nanofibers by electrospinning and their applications in nanocomposites. Composites Science and Technology, 2003. 63(15): p. 2223-2253.
45. Metrohm Autolab B.V. Autolab PGSTAT204 - Compact and modular potentiostat/galvanostat. 2016 [cited 2016; Available from: metrohm-autolab.com.
46. Fomin, G.S., et al., *Encyclopaedia of International Corrosion Standards*. 2003: Maney for the Institute of Materials, Minerals and Mining.
47. Talbot, D.E.J. and J.D.R. Talbot, *Corrosion Science and Technology*, Second Edition. 2007: CRC Press.
48. Sukiman, N.L., et al., Durability and Corrosion of Aluminium and Its Alloys: Overview, Property Space, Techniques and Developments. Aluminium Alloys - New Trends in Fabrication and Applications. 2012.
49. Khramov, A.N., et al., Hybrid organo-ceramic corrosion protection coatings with encapsulated organic corrosion inhibitors. Thin Solid Films, 2004. 447-448: p. 549-557.
50. Khramov, A.N., et al., Sol-gel-derived corrosion-protective coatings with controllable release of incorporated organic corrosion inhibitors. Thin Solid Films, 2005. 483(1-2): p. 191-196.
51. Instruments, G., Basics of electrochemical impedance spectroscopy. Gamry Instrument: Warminster, PA, USA, 2007.
52. Olivier, M.-G. and M. Poelman, Use of Electrochemical Impedance Spectroscopy (EIS) for the Evaluation of Electrocoatings Performances. 2012: INTECH Open Access Publisher.
53. Ecco, L.G., et al., EIS and in situ AFM study of barrier property and stability of waterborne and solventborne clear coats. Progress in Organic Coatings, 2014. 77(3): p. 600-608.
54. Tiwari, A., L. Hihara, and J. Rawlins, *Intelligent coatings for corrosion control*. 2014: Butterworth-Heinemann.
55. Bera, S., et al., Comparative Study of Corrosion Protection of Sol-Gel Coatings with Different Organic Functionality on Al-2024 substrate. Progress in Organic Coatings, 2015. 88: p. 293-303.
56. Criado, M., et al., Steel corrosion in simulated carbonated concrete pore solution its protection using sol-gel coatings. Progress in Organic Coatings, 2015. 88: p. 228-236.
57. Yu, M., et al., Effects of cerium salts on corrosion behaviors of Si-Zr hybrid sol-gel coatings. Chinese Journal of Aeronautics, 2015. 28(2): p. 600-608.
58. Sigma-Aldrich. 2016 june 10 2016]; Available from: www.sigmaaldrich.com.

Appendices

The following pages contain the poster presented on the *XIV Congreso Nacional de Materiales* in Gijón, the 8th, 9th and 10th June 2016 and the data sheets of the chemical compounds and equipment that has been used.

I. Appendix I: CNMAT 2016 poster



Estudio y diseño de recubrimientos nanoestructurados para la mejora del comportamiento a corrosión de aleaciones metálicas



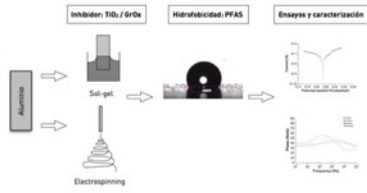
up^{na}
InaMat
Institute for
Advanced Materials

D. Maeztu¹, P.J. Rivero^{1,2}, C. Berlanga^{1,2} y R. Rodríguez^{1,2}

(1) Departamento de Ingeniería Mecánica, Energética y de Materiales (IMEM), Laboratorio de Materiales, Universidad Pública de Navarra (UPNA), Campus Arrosadía s/n, 31006, Pamplona, España. Contacto: maeztu.79067@e.unavarra.es
 (2) Instituto de Investigación en Materiales Avanzados (InaMat), Universidad Pública de Navarra (UPNA), Campus Arrosadía s/n, 31006, Pamplona, España.

Introducción

En este trabajo se ha llevado a cabo un estudio comparativo del comportamiento a corrosión de diferentes recubrimientos nanoestructurados obtenidos por dos técnicas de deposición. En la primera, proceso sol-gel, se han utilizado diferentes precursores alcóxidos (MTEOS, GPTMS y PFAS) para fabricar matrices a las que se les han añadido inhibidores de corrosión (TiO₂ y óxido de grafeno) y se han depositado por *dip coating* sobre probetas de aluminio 2024, en función de número de capas y tratamiento térmico. La segunda, *electrospinning*, se ha utilizado para fabricar un recubrimiento de fibras de espesor variable que contienen el inhibidor mediante el control de la viscosidad, potencial eléctrico, caudal y distancia de lanzado. Para evaluar el comportamiento a corrosión se han realizado estudios de espectroscopía de impedancias (EIS) y curvas de polarización mediante ensayos potenciodinámicos (voltametría). Además, se ha evaluado el comportamiento a corrosión de los diferentes recubrimientos en relación a su hidrofobicidad mediante la medida de los ángulos de contacto.



Parte experimental y resultados

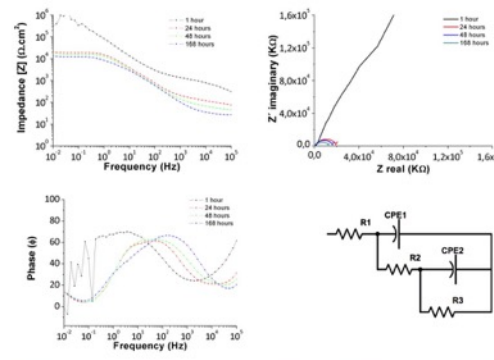


Figura: Diagramas de Bode del módulo y fase de impedancias y diagrama de Nyquist del recubrimiento de seis dips de GPTMS+MTEOS-óxido de grafeno. Circuito equivalente propuesto para el recubrimiento.

	R1 (Ω·cm ²)	CPE1 (F/cm)	α ₁	R2 (Ω·cm ²)	CPE2 (F/cm)	α ₂	R3 (Ω·cm ²)
1h	26.21	3.70E-07	0.68911	1453	1.84E-06	0.8559	6.96E+05
24h	43.13	1.38E-06	0.73817	112.4	7.50E-06	0.79259	20801
48h	30.8	1.73E-06	0.78304	52.31	8.86E-06	0.78206	17588
168h	11.36	1.96E-05	0.80356	12.57	2.76E-05	0.46405	6202

Tabla: Valores de los parámetros obtenidos a partir del circuito equivalente.

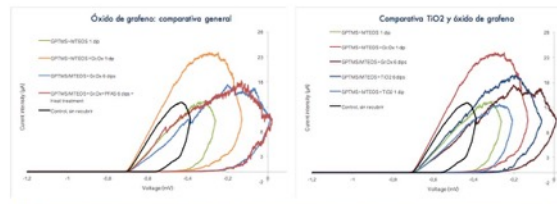


Figura: Comparativa de los ensayos de picadura de diferentes muestras y con diferente espesor de recubrimiento.

Muestra	Control, sin recubrir	GPTMS+MTEOS 1 dip	GPTMS+MTEOS +GrOx 1 dip	GPTMS+MTEOS +GrOx 6 dip	GPTMS+MTEOS +GrOx +PFAS 6 dip +HT.
Potencial de picadura [mV]	-0.57	-0.46	-0.40	-0.33	-0.29
Ángulo de contacto [°]	17.14	22.16	24.37	35.89	124.87

Tabla: Relación entre el potencial de picadura y el ángulo de contacto de las muestras con óxido de grafeno.

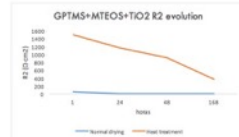


Gráfico: Evolución de la resistencia del recubrimiento en función del tratamiento térmico.

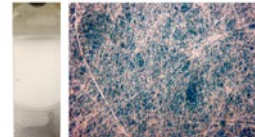




Imagen: Aluminio recubierta de fibras de electrospinning con TiO₂ y vista al microscopio.

Conclusiones

- Un aumento de la hidrofobicidad de la superficie (ángulo de contacto) conlleva mejor resistencia a la corrosión.
- Un tratamiento térmico posterior mejora las propiedades de resistencia a la corrosión, así como la estabilidad del recubrimiento.
- Los inhibidores de óxido de grafeno y dióxido de titanio mejoran las propiedades del recubrimiento a resistencia a la corrosión.
- El óxido de grafeno presenta propiedades anticorrosivas ligeramente superiores a las del dióxido de titanio.
- Es de gran importancia la insolubilidad en agua de las fibras de electrospinning resultantes.

Videos

- Recubrimiento de sol-gel por dip coating: 
- Recubrimiento por electrospinning: 

Agradecimientos

Los autores agradecen al Ministerio de Economía y Competitividad por la financiación de este trabajo a través del Proyecto TRA2013-48603-C4-1-R. También agradecen a la empresa Nadetech Innovations por el asesoramiento en el manejo de los equipos *ND-Rotatory coater* y *ND-ES Lab Electrospinning*. Por último, agradecen su colaboración al Departamento de Ingeniería Mecánica, Energética y de Materiales (IMEM) y al Laboratorio de Sensores de la Universidad Pública de Navarra.

Juan Deyo Maeztu Redin

85

II. Appendix II: Equipment and chemicals data sheets